Study on microphysical properties of midlatitude cirrus clouds observed by hydrometeor videosonde

（雲粒子ゾンデ観測による中緯度域巻雲の微物理特性に関する研究）

ORIKASA, Narihiro

（折笠　成宏）

A dissertation for the degree of Doctor of Science

Department of Earth and Environmental Sciences,

Graduate School of Environmental Studies, Nagoya University

（名古屋大学大学院環境学研究科地球環境科学専攻学位論文　博士（理学））

2015

ABSTRACT

Cirrus clouds are one of the most commonly occurring cloud types and cover over 20% of the earth's surface. Cirrus clouds have a strong impact on the global radiative energy balance by reflecting a part of incoming solar shortwave radiation back to the space and absorbing and reemitting longwave radiation. The net radiative forcing of cirrus clouds can be positive or negative depending on their radiative properties. The radiative properties are in turn controlled not only by macrophysical properties (cloud height, geometrical thickness, cloud fraction, cloud lifetime) but microphysical properties (number concentrations, shapes, size distributions of ice crystals, ice water content) of cirrus clouds. However, there is limited microphysical instrument that can reliably measure ice crystals smaller than 100 μm.

A new version of Hydrometeor Videosonde (HYVIS) for measuring cirrus clouds was developed. By adding a suction fan, sufficient sampling volume could be obtained to determine the form of size distributions at 250-m height intervals in cirrus clouds with low ice crystal concentrations. Theoretical calculation showed the collection efficiency of the new HYVIS should be unity for all ice crystals larger than 10 μm. On the basis of the comparison with concurrent data by other airborne instruments in the laboratory, the ice crystal concentrations can be measured by the HYVIS with an uncertainty factor of 2–3, although significant uncertainties are still included in the size range 10–30 μm. The reliability of the measured concentrations is supported by the observed size spectra of the dataset in this study and the simulated total concentrations of ice particles with a parcel model.

We have obtained the microphysical dataset which consisted of 37 launches from Tsukuba, Japan, during the observation period 1994–2007. The observational dataset of cirrus clouds was generally associated with a midlatitude warm front of a synoptic-scale

low, stationary (Baiu) front, or strong jet stream during spring to early summer. Vertical profiles of size distributions of cirrus cloud ice crystals were obtained for clouds with top temperatures ranging from −33° to −72°C and base temperatures from −3°C to −49°C.

Ice crystal concentrations varied approximately from the order of 10^{-1} to 10^{2} L^{-1}. Median ice crystal concentrations were typically several tens per liter regardless of temperature or their vertical location. While the concentrations were sometimes the highest near the cloud top, some clouds had their maximum concentration near the cloud base. As ice particles near the cloud base were usually in sublimation zones, it is suggested that crystal breakup through the sublimation process enhanced the concentrations in some cases. There was a large difference between the measured concentrations and simulated ones in earlier modeling studies of cirrus cloud formation that treated the ice crystal generation process through homogeneous ice nucleation of aqueous solution droplets, although the measured ones are probably affected by other physical processes such as secondary ice formation and gravitational sedimentation and turbulent mixing of ice particles after the initial cloud formation. Furthermore, a strong temperature dependence expected from heterogeneous ice nucleation formulas at relatively warm temperatures (>−25°C) was not found over all temperature ranges. Although it is difficult to determine which was dominant for ice initiation process in observed clouds, homogeneous nucleation or heterogeneous nucleation, some implications for ice nucleation mechanisms in cirrus clouds in comparison with recent modeling studies involving heterogeneous ice nucleation at temperatures below −40°C are discussed.

The contribution of small ice crystals (<100 μm) to the mass or extinction (or area) in observed cirrus clouds was examined. The averaged contribution in size of $D < 50$ μm tended to decrease as the total mass or area became larger, while that in size ranges of $D > 100$ μm tended to increase; the contribution to the total in size range of $100 < D < 200$

μm became most dominant for larger mass and for larger area. In the HYVIS dataset, the small ice crystals had little impact on the mass or extinction in cirrus clouds, compared with results of the previous studies.

The frequency of the occurrence of ice crystal habits in the HYVIS dataset was investigated. The predominant types were single bullets at temperatures ranging from –60° to –20°C. Plate-type crystals were dominant at temperatures warmer than –20°C, whereas column or bullet rosette crystals became dominant at temperatures colder than –60°C. The distributions of the ice crystal habits derived from the HYVIS observations were consistent with the results of recent laboratory and field experiments, although the dependency of the ice crystal habits on ice supersaturation was not characterized in this study because only limited accurate humidity data were available under low temperature conditions.

The size dependency of the distributions of the axis ratios of column and bullet crystals tended to decrease with increasing crystal dimension. We found no clear temperature dependency of the axis ratios of columnar crystals. The area ratios of classified crystal habits were found to be comparable with previously reported ratios. The fact that the area ratio decreased with increasing dimension was apparent for all crystal types. Polynomial curves fit to plots of area ratio versus maximum crystal dimension for each crystal type evidenced patterns different from those reported in previous studies. When the conventional power–law relationships between cross-sectional area and dimension reported in a previous study were applied to the HYVIS data, we found that the power-law relationships could overestimate the measured cross-sectional area integrated over the 250–m height interval between the cloud base and the cloud top by 10%–80%.

TABLE OF CONTENTS

1. Introduction

High-level ice clouds are one of the most commonly occurring cloud types and cover over 20% of the earth's surface (Barton, 1983). They are thought to strongly influence the global energy budget by modifying infrared radiation emitted from the earth's surface, and consequently, have a great impact on climatic change (e.g., Liou, 1986). In order to understand the climate system, it is necessary to increase our knowledge about microphysical, radiative, and optical properties of cirrus clouds. To understand their radiative properties, it is critical to know the size distributions within these clouds and measure of their radiatively effective size (Stephens et al. 1990), as well as crystal shape (Mishchenko et al. 1996). In situ measurements on microphysical structures of cirrus clouds have been performed using special, high-altitude flying aircraft. Two-dimensional optical array probes, which are often used for aircraft measurements of cloud particles, do not have sufficient resolution to discriminate between cloud droplets and ice crystals whose sizes are smaller than about 100 μm, and cannot detect details of crystal habits.

To overcome these difficulties, the cloud physics group in Meteorological Research Institute (M.R.I.) had developed balloonborne special sondes; a Cloud Particle Video Sonde (a prototype of Hydrometeor Videosonde) by Murakami et al. (1987) and a Hydrometeor Videosonde (HYVIS) by Murakami and Matsuo (1990). Earlier HYVIS cirrus cloud observations (Mizuno et al., 1994) showed sampling volume requires to be increased in cirrus clouds with low ice crystal concentrations. Moreover, the weakness of downward scattered light degraded the quality of particle images, making it necessary to change the illumination from natural light to artificial, controlled light. To meet these requirements, we have built a new version of the HYVIS.

The balloonborne observation of vertical penetration through clouds with the HYVIS can be one of the most useful techniques for in-situ cloud measurements. One major advantage of a balloonborne instrument over other microphysical instruments is the

accessibility not only to low orographic clouds and/or severe convective clouds (where research aircraft can hardly be operated due to safety regulations) but also to the highest clouds such as cirrus clouds (that are difficult to access for most of propeller research aircraft). The second advantage is that the HYVIS can take images in sufficient resolution to distinguish between cloud droplets and ice crystals whose sizes are smaller than 100 μm, and can detect habits of such ice crystals. The third advantage is that the HYVIS can obtain vertical distributions of hydrometeors at fine resolution.

Firstly, this study focuses on an examination of the concentrations of ice crystals in cirrus clouds, a microphysical variable of cirrus clouds that has been difficult to quantify in the past. While the number concentrations seem to have no direct link with the radiative properties of cirrus clouds, given an ice water content as measured from an aircraft or inferred from radar measurements, the concentrations and size distributions affect the “effective diameter” for cloud extinction, extinction coefficient, and cloud optical depth.

Airborne impactors (e.g., replicators, video ice particle samplers) have been used to quantify the concentrations of small ice particles in cirrus (e.g., Hallett 1976; Heymsfield and McFarquhar 1996; Schmitt and Heymsfield 2009). Measurements of ice crystal concentrations from airborne impactors can be unreliable because the larger crystals can breakup on their impactions at high speeds attained by an aircraft. Furthermore, the efficiencies at which impactors collect small ice particles have not been fully characterized either experimentally or numerically. The cloudscope developed by the Desert Research Institute (Schmitt and Arnott 1999), which is also an airborne cloud probe and has been used for detecting particles ranging from 3 to 400 μm, has a feature of heating the microscope objective to prevent buildup of ice particles. Because it is difficult to estimate the geometry of the cloudscope, the collection efficiency for ice particles has not been intensively studied.

The cloud particle imager (CPI) probe developed by SPEC Inc., provides high-quality digital images for particles >10 μm in diameter, and no airspeed correction is needed for most research aircraft (up to 200 m s^{-1}) because of the fast electronic response time of the pulsed illumination and the CCD camera (Lawson et al. 1998a, 1998b), which is one of the main advantages. Lawson et al. (2001) reports a few methodologies to calculate particle concentrations; however, the sample volume for small particles (<20 μm) may still need to be investigated because of uncertainty in the detection threshold level of the CPI particle detection system, which directly affects its counting efficiency. In a recent study by Connolly et al. (2007), the errors in particle sizing and definition of the depth of field were assessed to propose a correction algorithm for particle size distributions measured with the CPI. The 2D-S (Stereo) probe, recently developed by SPEC Inc., is an optical array imaging instrument utilizing two laser beams with a newer technology that supports high-resolution (10 μm) and fast-time response (Lawson et al. 2006c); resizing of out-of-focus images and counting efficiency for small particles (<100 μm) are significantly improved over older optical array probes. The effects of ice particle shattering on the arm tips for the 2D-S measurements need to be investigated in a comprehensive manner, even when the interarrival time algorithm for a particle appears to be more effective in mitigating the shattering effect than the modified probe tips (Lawson 2011).

The Particle Measuring System (PMS) imaging probes have been frequently used for measuring ice crystal size distributions. The PMS two-dimensional cloud probe (2DC) can only obtain reliable estimates of the concentrations down to a size of approximately 125 μm on the basis of an assessment of the probe's performance in the wind tunnel experiment (Strapp et al. 2001). For smaller ice particles, a forward scattering spectrometer probe (FSSP) has been used in a number of studies. However, estimates of the concentrations of the small particles are uncertain because larger crystals can contribute to the concentrations of the FSSP (Gardiner and Hallett 1985) and the optical

scattering characteristics of the ice particles are not clearly known (Heymsfield and Platt 1984). On the other hand, studies show that the FSSP could make reliable measurements for some types of cirrus clouds, such as contrail cirrus, cirrus outflow from hurricane, or arctic cirrus, where quasi-spherical small crystals were dominantly found and few large crystals were present (e.g., Gayet et al. 1996; Lawson et al. 2001; Ivanova et al. 2001). However, as pointed out by Gayet et al., the FSSP measurements can be quite unreliable for accurate sizing and counting ice particles in natural cirrus with large nonspherical ice crystals or relatively broad size distributions. Field et al. (2003) evaluated the effect of ice particle shattering on the FSSP inlet by analyzing the interarrival times for ice crystals and showed that the ice crystal concentrations measured in midlatitude cirrus could be overestimated typically by a factor of about 2 (by as much as a factor of 5 in the worst case). This issue of ice shattering holds true for the standard arm tips or inlets of the other airborne in situ probes for detecting ice crystals, such as 2DC, 2D-S, cloud imaging probe (CIP), and cloud and aerosol spectrometer (CAS). The artifacts for optical imaging probes can be mostly corrected in some cases on the basis of the particle interarrival times (Field et al. 2006) or significantly mitigated by using modified tips (Korolev et al. 2011). However, a more comprehensive study is required for quantifying the effect of shattering on airborne in situ measurements, which is expected to depend on multiple factors including particle size and type (density, habit), airspeed, angle of attack, probe geometries and depth of field, and cloud conditions.

Balloonborne instruments can have the ability to measure the concentrations of small ice particles as their strength because minimal crystal breakup occurs at their ascent speed and they are designed to have a minimum detection threshold of 5–10 μm. The hydrometeor videosonde (HYVIS) (Murakami and Matsuo 1990; Orikasa and Murakami 1997) and the balloonborne ice crystal replicator (Miloshevich and Heymsfield 1997) are two types of balloonborne instruments for cirrus cloud microphysical measurements.

However, for these instruments, the collection efficiency decreases to sizes below 10 μm, so few tiny crystals are actually sampled. More importantly, detailed analysis of the collection efficiency is needed for the impactor-type instruments with different flow fields and sample inlet systems because the dependence of the collection efficiency on particle size might be strongly influenced by deviations from a simplified theoretical approach, as suggested by Miloshevich and Heymsfield (1997).

It is difficult to directly detect ice crystal nucleation in cirrus clouds; the observed properties of cirrus clouds do not describe the conditions at the time of crystal generation. In contrast, wave clouds enable us to observe successive stages in the ice nucleation process (Heymsfield and Miloshevich 1993). Aircraft measurements in orographic wave clouds have been used to investigate ice nucleation processes at low temperatures (over the range from −30° to −56°C), and the results from wave cloud studies have been used to gain a better understanding of the ice formation and evolution processes in cirrus clouds (Heymsfield and Miloshevich 1993, 1995). The measurements were consistent with the scenario by numerical modeling that involves the formation and growth of haze particles and subsequent homogeneous freezing. Homogeneous ice nucleation was introduced as a means of explaining the presence of liquid water supercooled to −36 °C and its absence at temperatures below −36 °C (Sassen and Dodd 1988, 1989; Heymsfield and Sabin 1989). Jensen et al. (1998) also compared in situ measurements in wave clouds with numerical simulations. The observed peak ice crystal concentrations and peak relative humidities were consistent with the simulated values at moderate to high updraft velocities (1–4 m s^{-1}) for wave clouds. The rate of ice production by homogeneous nucleation depends strongly on the updraft velocities (DeMott et al. 1994). Because the vertical velocities in the wave clouds studied by these researchers were one or more meters per second, the homogeneous ice nucleation process is interpreted as a dominant ice nucleation mechanism within vigorous convection and updrafts of cirrus clouds.

DeMott et al. (1994) have studied the interplay of homogeneous versus heterogeneous ice nucleation processes in cirrus clouds conducting sensitivity studies with a Lagrangian parcel model and with a 2D version of a mesoscale cloud model (CSU/RAMS). They found that the cloud condensation nucleus (CCN) and ice nucleus (IN) profiles in the vertical (with temperature) have a profound effect on which ice nucleation mechanism is dominant. They also found that heterogeneous nucleation dominates when the updraft velocities are low, which corresponds to cirrus clouds associated with synoptic-scale ascent, and leads to relatively low ice crystal concentrations (of the order 10 to 100 L^{-1}). With vigorous updrafts, homogeneous nucleation (freezing) of cloud and solution droplets dominates and leads to concentrations as large as several tens per cubic centimeter.

Box model studies (e.g., Gierens 2003) suggest that the suppression of homogeneous ice nucleation depends on environmental conditions (including updraft velocities) as well as the amount of heterogeneous ice nuclei. Within the framework of a 2-D nonhydrostatic model, the process of ice particle sedimentation, which is usually not implemented in box models, can be incorporated for the investigation of the effect of both ice nucleation mechanisms on the life cycle of cirrus clouds (Spichtinger and Gierens 2009). Such recent modeling studies introduce new insights and implications on the interplay of nucleation mechanisms in natural cirrus clouds.

Secondly, this study focuses on the importance of small ice crystals (<100 μm) to the mass or extinction in cirrus clouds. In previous studies, contradictory conclusions on that issue have been reached. The dataset obtained from the FSSP or CAS instrument generally showed the substantial contributions of small crystals to the radiative properties (e.g., Ivanova et al. 2001; Garrett et al. 2003). The common aspect of the above datasets is that the airborne in-situ instruments ingest ice crystals through an inlet and are flown on jet aircraft at high airspeeds, leading to the cause of small-particle artifacts due to shattering of large ice crystals. Recent studies have been performed using the

other types of airborne instruments (Cloud Droplet Probe (CDP) or 2D-S) to compare with the concurrent data with the FSSP or CAS, which concluded that the small crystals had less impact on cirrus extinction (McFarquhar et al. 2007; Jensen et al. 2009). Although further investigations are still required to reevaluate the importance of the small ice crystals in previous studies, it is important for reliable estimation of radiative properties in cirrus clouds to quantify the contributions of those crystals to the mass or extinction measured with more reliable instruments.

Thirdly, this study focuses on an examination of the habit of ice crystals in cirrus clouds, which is one of the least known but most complicated factors needed to quantify the impact of cirrus clouds on climate, because the crystal shape determines the terminal velocity, projected cross-sectional area, and ice water content of ice particles. Moreover, the distribution of ice particles of different shapes affects the lifetime, scattering properties, and growth rates of precipitation in ice clouds.

Cirrus clouds consist of ice particles with a variety of shapes and sizes; the sizes of the particles range from <10 μm to a few millimeters. The distribution of ice crystal shapes and sizes in cirrus clouds could have a significant impact on the sign (warming or cooling) of cirrus cloud net radiative forcing (Zhang et al. 1999). To improve parameterizations for cirrus radiative properties in climate models, it is important to accurately quantify the single scattering properties of the individual particles with a given size and shape. Kristjánsson et al. (2000) have demonstrated that ice crystal size and shape may have a significant influence on climate changes projected by global climate models.

Many studies have focused on the radiative impact of nonspherical ice crystal habits on the solar part of the electromagnetic spectrum (Mitchell and Arnott 1994, hereafter MA94). Wendisch et al. (2005) concluded that the impact of cirrus ice crystal shape on solar spectral irradiance was important with respect to reflected irradiance above an optically thin cirrus cloud, especially for small solar zenith angles. Few studies have been

conducted about the thermal IR part of the spectrum to evaluate the influence of ice crystal habits on thermal IR cirrus radiative properties (Francis et al. 1999). Wendisch et al. (2007) concluded that the effects of cirrus ice crystal shapes on thermal IR irradiance were substantial for high, optically thin cirrus clouds, especially with respect to upwelling irradiance above the clouds.

An early study of in situ observations of cirrus clouds was conducted by Weickmann (1947), who revealed that in convective cirrus clouds the primary ice crystal type was a bullet rosette consisting of hollow prismatic crystals in three-dimensional clusters, and in cirrostratus clouds the primary ice crystal types were single bullets, columns, and thick plates. Heymsfield and Platt (1984) collected replicator data from cirrus clouds and determined the predominant crystal types in several temperature ranges. At temperatures between –20° and –40°C, they observed spatial or polycrystalline forms with some columns, plates, and bullets. At temperatures between –40° and –50°C, the predominant crystal types were hollow columns and spatial forms in stable and convective cirrus clouds, respectively. At temperatures below –50°C, the predominant types were hollow or solid columns with some hexagonal plates, although bullet rosettes were occasionally observed.

Recent field observations have advanced our knowledge of ice crystal shapes in clouds. Extensive observations with the cloud particle imager (CPI) have been conducted in several field campaigns (Lawson et al. 2001; Baker and Lawson 2006; Lawson et al. 2006a, 2006b) and have targeted several types of clouds: wave clouds, midlatitude and high-latitude cirrus clouds, tropical anvil and cirrus clouds, and arctic clouds. These studies suggest that midlatitude and high-latitude cirrus clouds may be comprised of more “rosette-shaped” crystals (polycrystals with a rose shape, including budding rosettes with short arms, mixed-habit rosettes, or rosettes with plate-like/side-plane features) than previously reported.

Laboratory experiments reveal that the ice crystal habit and its size are governed by temperature and ice supersaturation. Recent laboratory studies have provided a comprehensive description of ice crystal habits in the atmosphere at temperatures ranging from 0° to –70°C (Bailey and Hallett 2004, 2009, hereafter BH04 and BH09). These results, supported by recent observational studies, have confirmed that the crystal habit in the atmosphere at temperatures between –20° and –40°C is dominated by plate-like polycrystalline forms. In the lower temperature ranges (<–40°C), the crystal habit regime is shifted to columnar polycrystalline forms.

The terminal velocity, extinction coefficient, and effective radius of ice particle are related to the projected cross-sectional area that depends on particle size and shape. Most studies have used habit-dependent relationships between ice particle diameters (maximum dimensions) and cross-sectional areas to estimate the total area of a population of particles (Mitchell 1996; Mitchell et al. 1996, hereafter M96 and Me96, respectively). However, the appropriateness of such empirical equations is uncertain, and the estimation error should be examined on a case-by-case basis. Heymsfield et al. (2002) proposed a general approach for improving the derivation of microphysical properties (bulk density and mass of ice particles) of ice clouds on the basis of two parameters: the maximum dimension and the projected cross-sectional area of the ice particle. Recently, cross-sectional area data from past studies have been evaluated and parameterized for each crystal shape by introducing a shape-sensitive parameter, the area ratio (Heymsfield and Miloshevich 2003, hereafter HM03).

Most microphysical, in situ data from previous studies have been obtained from aircraft observations. Balloonborne hydrometeor videosonde (HYVIS) (Murakami and Matsuo 1990; Orikasa and Murakami 1997) has some advantages over aircraft observations for cirrus cloud observations. A HYVIS can easily reach the highest clouds — up to the top of cirrus clouds — and has sufficient resolution to distinguish the shapes

of ice particles smaller than 100 μm. The HYVIS can obtain the vertical distributions of hydrometeors at fine spatial resolutions and with relatively few artifacts, such as shattering and breakup, compared with aircraft observations. The datasets from in situ observations are still limited, although a variety of microphysical instruments have been developed and used for many years.

The outline and improvements in the new HYVIS are described in section 2. The dataset and examples of cirrus cloud observations are presented in section 3. In section 4, we report on the concentrations of ice crystals measured by the HYVIS in cirrus clouds generally associated with warm or stationary fronts of synoptic-scale lows, basic to the study of cirrus cloud properties and ice nucleation processes in the atmosphere. From these observations, we speculate on some aspects of the nucleation processes. Contributions of small ice crystals to total mass or area in cirrus clouds measured with the HYVIS are reported in section 5 to briefly assess the importance of small ice crystals. In section 6, we report the frequency of the occurrence of ice crystal habits in midlatitude cirrus clouds that were generated primarily by synoptic-scale systems. The measurements were performed using a balloonborne HYVIS. The distributions of the axis and area ratios of ice particles in our dataset are presented for comparison with results of previous studies. The characteristics of ice crystal habits and shape-sensitive parameters in the HYVIS dataset are discussed, and the results are compared with other observational datasets and laboratory studies.

2. Development of instrument

2.1 Outline of new HYVIS

Figure 2.1 shows a photograph of the new HYVIS. Its weight is approximately 2.4 kg, which is about 1 kg heavier than the original HYVIS as a result of adding a suction fan and an associated battery. A cut-out view of the new HYVIS is shown in Fig. 2.2. The dimensions of the new HYVIS are 280 mm × 106 mm × 500 mm, including the electric light for microscope. It has two video cameras (Sony HVM–52H) with different magnifications to take pictures of hydrometeors from 7 μm to 5 mm in size; they are referred to as close-up camera and microscopic camera, and the areas of each image are 5.48 mm × 4.04 mm and 1.79 mm × 1.32 mm, respectively. Hydrometeors are sucked through a particle inlet of 1 cm in diameter and collected on a surface of transparent 35 mm leader film (Fuji Photo Film Co.) over which silicone oil (KF96, Shin-Etsu Chemical Co.) is applied. Examples of HYVIS images with two video cameras are presented in Fig. 2.3.

Two types of images are transmitted alternately with a period of about 10 seconds. For the first 6 s, the microscopic camera takes pictures of ice crystals of the order of 10 to 100 μm in size. At the beginning of the shooting of the close-up camera, the film is moved at a distance between the two cameras. Then the close-up camera takes pictures of larger ice crystals of the order of 100 μm to 1 mm for another 4 s.

The ground receiving system for the new HYVIS is the same as for the original HYVIS. Images of hydrometeors taken by two small video cameras are transmitted by 1687 MHz microwave to a ground station in real time so that it does not need to be retrieved later. At the same time, meteorological data are transmitted at a frequency of 1673 MHz.

2.2 Description of the improvements

As shown in Fig. 2.2, the new HYVIS with a small suction fan (V484M, Micronel)

forces hydrometeors to fall through the particle inlet (nozzle with a section area ratio 4:1 between the top and the base). The velocity of air flow under the condition of normal temperature and 1000 hPa is approximately 12 m s^{-1} at the base of the impactor nozzle, which corresponds to a flow rate of about 1 L s^{-1}, five times as voluminous as the rate of the original HYVIS (natural ventilation type). The addition of the fan makes the following devices necessary:

(a) Coating silicone oil on the sampling film to prevent ice crystals from bouncing off.

(b) Precise movements of the film from the sampling position (the position over the microscopic camera) to the position over the close-up camera.

(c) Monitoring changes in flow rates with environmental conditions.

Silicone oil is gradually released on to the film through leakage holes from a silicone oil reservoir, and is spread thinly and uniformly with the help of a wiper blade. Silicone oil is pushed out from the reservoir by expanding air in the reservoir as the HYVIS ascends and ambient pressure decreases; this is the same mechanism as that replica solution is released on to the film in the snow crystal sonde (Magono and Tazawa, 1966). Since the viscosity of silicone oil increases as temperature decreases, silicone oil with low viscosity (*e.g.*, 20 cSt) is used.

Accuracy of film movement was improved by adopting a winding mechanism that controlled the rotation angle of the sprocket instead of the rotation time. It is confirmed that the accuracy of the distance was 35.6 ± 1.5 mm at ground tests. A microphoto sensor for detecting reflected light from one of fan blades is used to monitor rotation rates. While the winding motor is working (about 1 s), an LED blinks every 60 rotations of the fan. The blinking motions are projected on to close-up images, from whose periods the rotation rates can be estimated.

In order to get higher quality images of ice crystals in cirrus clouds where downward scattered light is weak, the illumination for the close-up camera was changed from

natural diffused light to a bundle of LED lamps with a diffusion plate. This method of illumination ensures particle images in sharp contrast with the background. This modification also makes nighttime observations possible.

2.3 Determination of the sampling volume and the collection efficiency

In order to deduce number density of ice crystals from the number of them collected on the film, it is necessary to estimate the flow rate of air and the collection efficiency for ice crystals.

First, we examined the relation between the rotation rates of the fan and the flow velocity. Figure 2.4 shows a linear relationship between them. Experiments in a decompression chamber were carried out to estimate the flow rate at altitudes where cirrus clouds occur. The flow velocity v was estimated from the measurements of differential pressure ΔP between the particle inlet and the surroundings using the following relation:

$$\Delta P = \frac{1}{2}\zeta \rho v^2 , \tag{2.1}$$

where ρ is the density of air and ζ is the unique coefficient of pressure loss by the duct. When the cross section of the duct changes gradually and the pressure loss by fluid friction is negligible, ζ can be assumed to be unity. Figure 2.5 shows the relation between the ambient air pressure and the flow velocity v at three different rotation rates of the fan (10000, 6000, and 2000 rpm). The differential pressure decreases with decreasing atmospheric pressure, which makes the degree of error more serious as shown by error-bars in Fig. 2.5. The flow velocity did not change significantly with atmospheric pressure at a constant rotation rate of the fan until the pressure was reduced to about 200 hPa, which commonly corresponds to the altitude of cirrus cloud tops. Although, beyond 200 hPa, it was difficult to exactly estimate the flow velocity, it is suggested that

the flow velocity should be constant at altitudes where cirrus clouds occur. Since the relation between the rotation rates and the flow velocity is linear, monitoring the rotation rates by using the microphoto sensor enables us to evaluate the flow rate.

Ascent velocities of the new HYVIS are another factor which has an influence on the flow velocity. During the ascent of the HYVIS, ambient air flow accelerates the air that goes through the nozzle. Figure 2.6 shows the relation between the ambient air speed U_∞ and the flow velocity *v* at the nozzle base obtained from wind tunnel experiments. In both the case (a) and the case (b), the flow velocity has a tendency to increase linearly with increasing U_∞ except for smaller values of U_∞. It is found from the experimental data of case (b) that the linear relation between *v* and U_∞ holds when ambient air speeds are higher than the flow velocities at the nozzle top and otherwise v is insensitive to U_∞. Experimental data at smaller values of U_∞ are not available for the case (a). The inconsistency of flow velocities between cases (a) and (b) is supposed to result from slightly different inner shapes of two units of the new HYVIS used, particularly the clearance between the nozzle base and the film surface. Ascent velocities of the new HYVIS change within the range of air speeds where the linear relation is satisfied. Therefore the following linear relation, derived by interpolating the two relations for the cases (a) and (b), will be used to estimate the flow velocity at the nozzle base:

$$v = (0.88v_5 - 2.74) + (0.025v_5 + 0.55)U_\infty \ , \qquad (2.2)$$

where v_5 is the flow velocity at U_∞ = 5 m s^{-1}.

To determine the collection efficiency (*CE*) of the new HYVIS for ice crystals, a calculation was carried out on the basis of the collection efficiency of particles determined by Ranz and Wong (1952) for round jets. This treatment needs to estimate the correction factor for Stokes drag. For Reynolds number less than 0.01, the correction factor for non-spherical particle has not been determined. However, this factor was estimated by

extrapolating the experimental results obtained at larger Reynolds numbers. The assumption is made here that the shapes of hexagonal plates and hexagonal cylinders can be approximately expressed by oblate spheroids and circular cylinders, respectively. Figure 2.7 shows the calculated collection efficiencies of spherical droplets, hexagonal plates (aspect ratio 0.2), and hexagonal cylinders (aspect ratio 2) as types of collected particles, under the condition where the atmospheric pressure is 200 hPa and the flow velocity at the nozzle base is 12 m s^{-1}. For both the hexagonal plates and the hexagonal cylinders, the *CE* of the HYVIS is unity when their maximum sizes are larger than 10 μm. Since the aspect ratios of nascent ice crystals around 10 μm in size are considered not to deviate greatly from unity, it is reasonable from this theoretical approach to assume that all ice crystals larger than 10 μm are collected.

To confirm the actual *CE*, we have recently conducted calibration experiments in our laboratory with small particles by comparing with the concurrent data of other instruments. The Appendix-A describes such comparison and uncertainty in the HYVIS measurements. Although currently there is neither a standard instrument nor a standard technique for number concentration measurements of cloud particles, the calibration experiments here should be regarded as a reference. We estimated from the comparison that the number concentrations of ice particles in the size range 10–100 μm measured with the HYVIS would be accurate within only a factor of 2 to 3 partly owing to the uneven distribution of actually collected particles on the suction area. In contrast to the HYVIS, large uncertainties still remain in the number concentrations of particles smaller than 50 μm for currently available airborne instruments owing to errors caused by ice particle shattering and sample volume uncertainties (Baumgardner et al. 2012).

The comparison with other microphysical instruments (see Appendix-A) suggested that the *CE* of the HYVIS had the uncertainty within a factor of 2 to 3 for 10–30 μm particles and with a factor less than 2 for particles larger than 30 μm. In this study we

assumed the CE was unity for all particles actually collected because further data are still required to establish the correction of CE as a function of particle size.

Fig 2.1 Photograph of the new version of HYVIS.

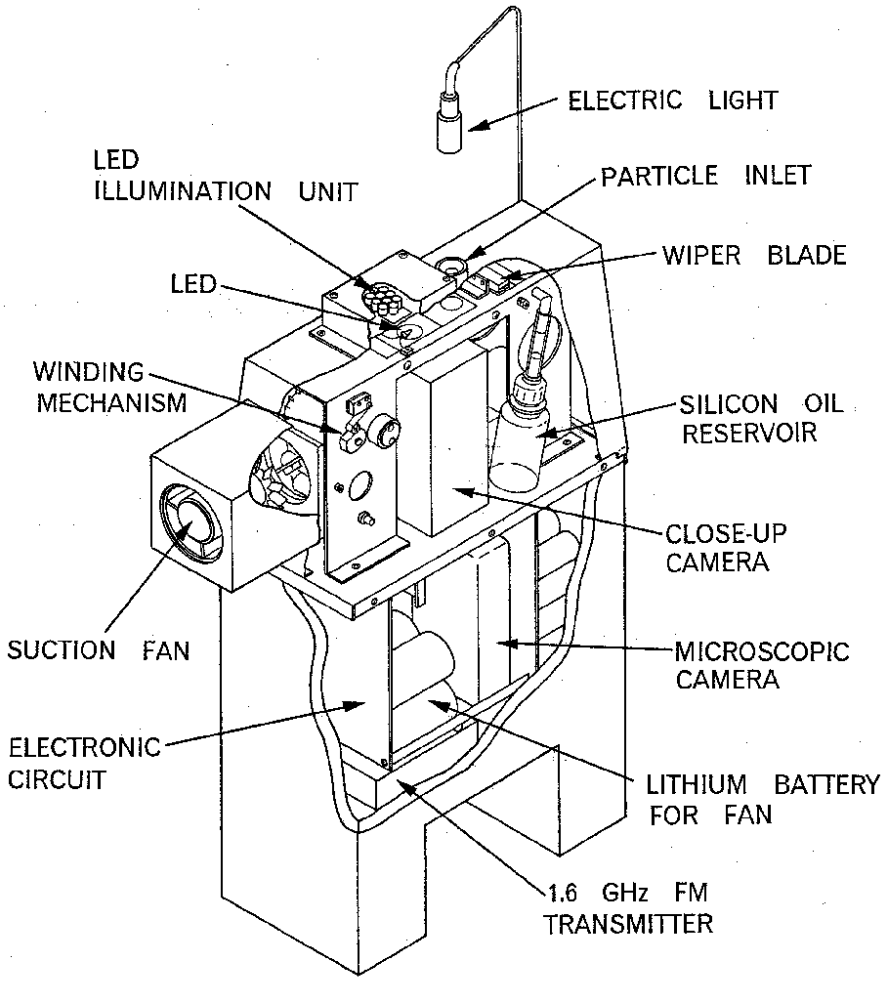

Fig 2.2 Cut-out view of the new HYVIS.

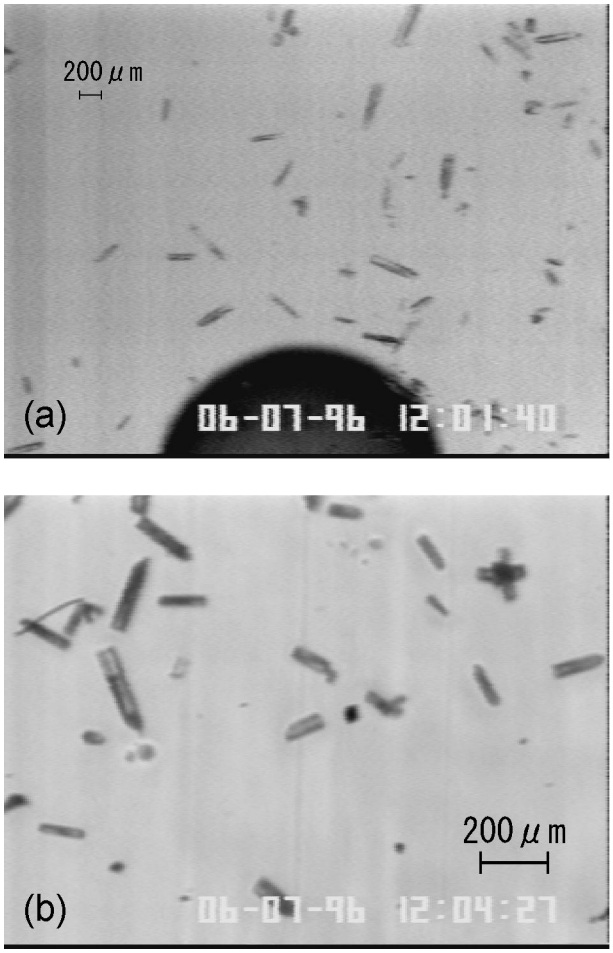

Fig 2.3 HYVIS images taken with a close-up camera (top) and a microscopic camera (bottom).

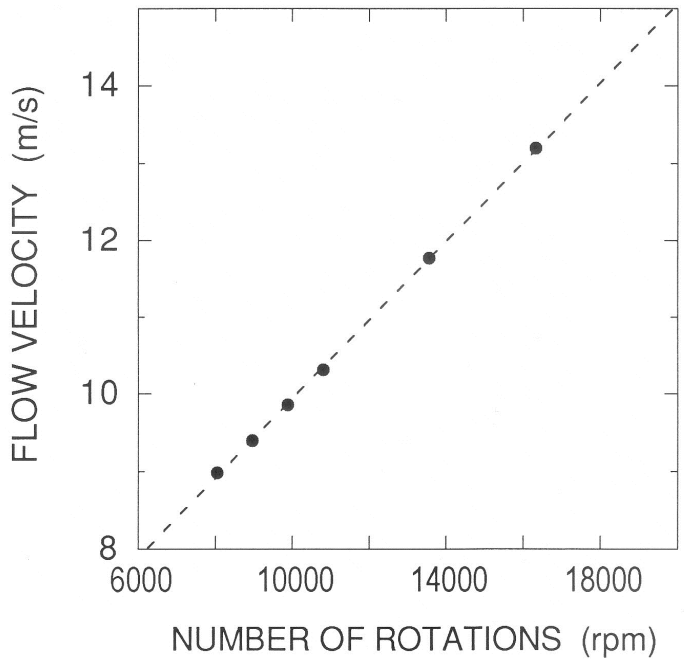

Fig 2.4 Relationship between rotation rates of a fan and flow rates of air.

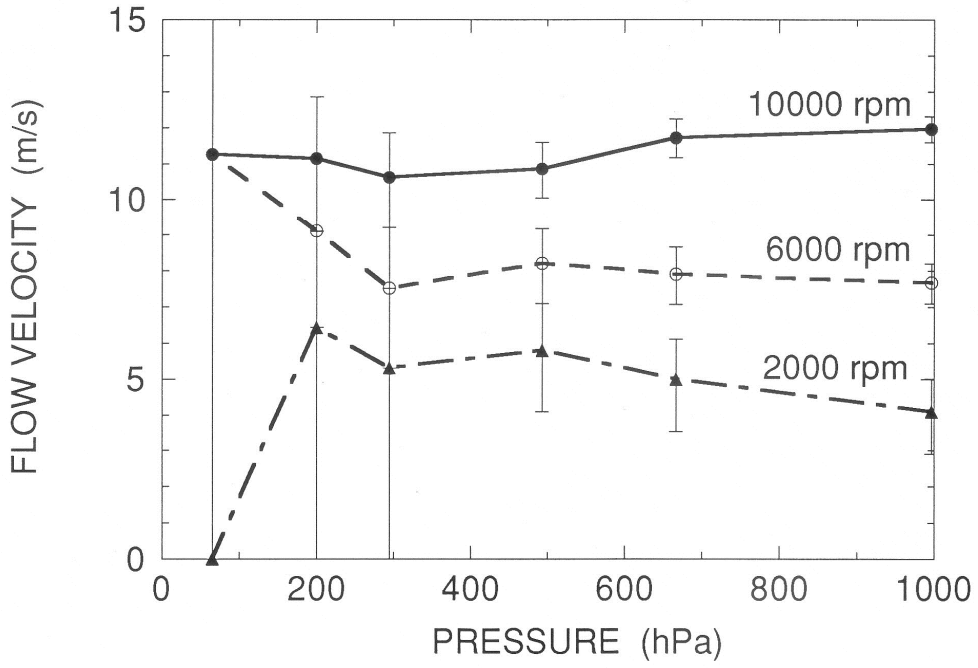

Fig 2.5 Dependence of the flow velocity on ambient pressure at three different rotation rates of the fan. Vertical solid lines indicate the magnitude of errors in measurement of the velocity.

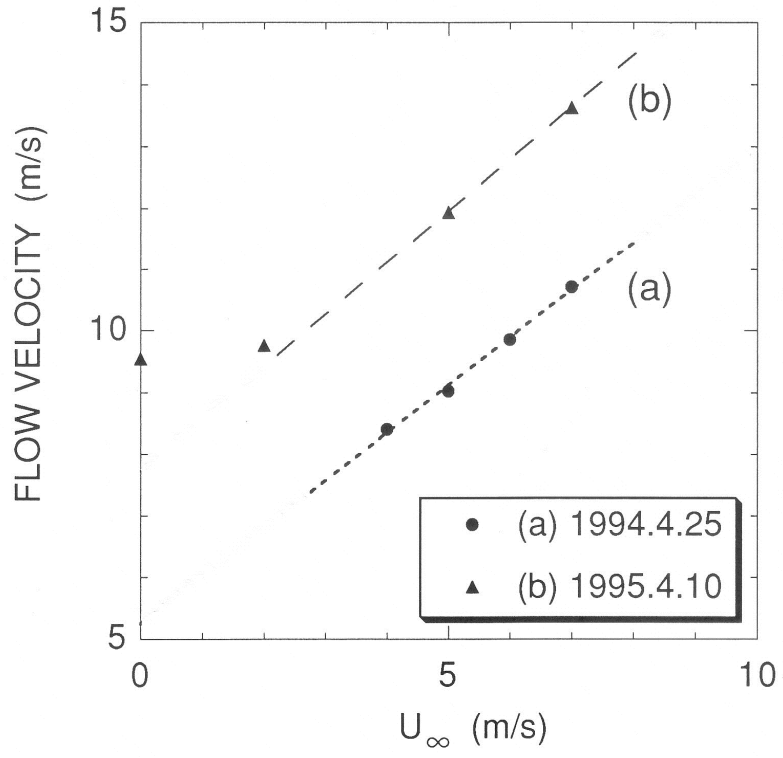

Fig 2.6 Change in the flow velocities with ambient air speed (U_∞).

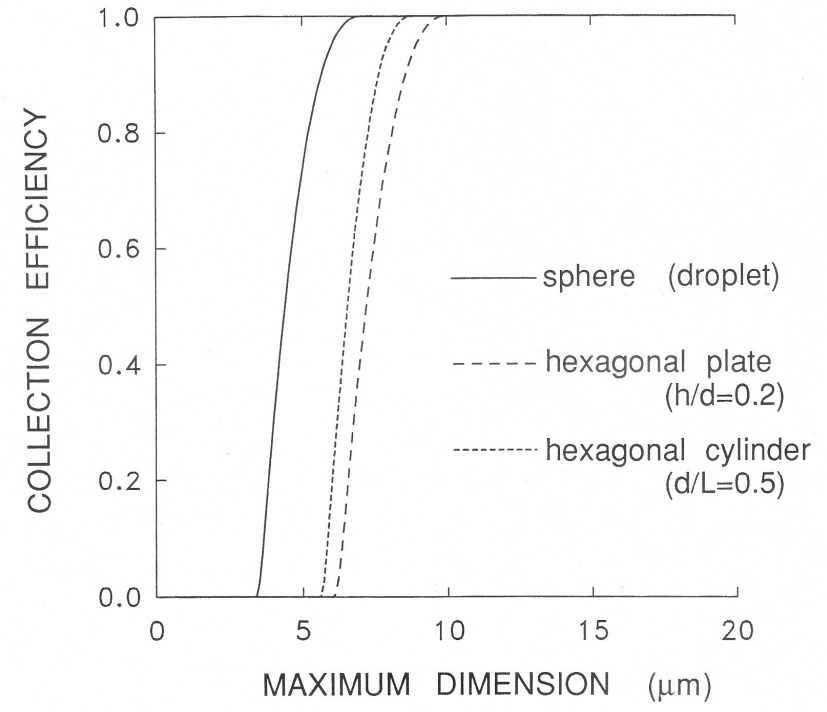

Fig 2.7 Calculated collection efficiencies of the new HYVIS for cloud particles at 200 hPa at a flow velocity of 12 m s^{-1}. Shapes of particles treated are spherical droplet (solid line), hexagonal plate (long-dashed line, h/d=0.2), and hexagonal cylinder (short-dashed line, d/L=0.5), where h and L refer to the thickness of plates and the length of cylinders, respectively, and d is the diameter of circle circumscribed to basal plane of ice crystals.

3. Dataset and examples of cirrus cloud observation

3.1 HYVIS Dataset

The cirrus cloud microphysical dataset was collected by the HYVIS during the period 1994–2007. We have successfully acquired and analyzed the imagery for 37 launches of the HYVIS, consisting of about 4600 video images of ice particles in cirrus clouds, in 1994–1999 as part of the Japanese Cloud and Climate Study (JACCS) field program and in 2003–2007 as post-JACCS field campaigns. The JACCS cirrus experiment was conducted from Tsukuba (36.0°N, 140.1°E), Japan. The ground-based observational system consisted of a special sonde (HYVIS + radiation sonde) system, a cloud lidar, a windprofiler, and various types of spectroradiometers (Asano et al. 1997). In the post-JACCS campaigns, the limited instruments, lidar and radiometers as well as the HYVIS, were operated.

We have obtained the observational dataset of cirrus clouds generally associated with a midlatitude warm front of a synoptic-scale low, stationary (Baiu) front, or strong jet stream during spring to early summer (from March to July, mostly in May and in June). The dataset contained herein was obtained from mostly cirrostratus and/or cirrus, identified by a trained meteorological observer on the basis of a cloud atlas (WMO 1975), while in about 20% of all cases, cirrostratus was linked together with altostratus (no water droplets from the HYVIS imagery) so that it was difficult to identify the line between two types of cloud. Although the definition of a cirrus cloud needs to be carefully considered in order to determine its climatology (Sassen and Campbell 2001), we consider it reasonable to regard all our data as cirrus clouds on the basis of comparison with other datasets (Dowling and Radke 1990). Besides, neither case of precipitation nor anvil clouds from deep convection was included in the dataset studied here. There were no in situ aircraft measurements and cloud radar data available.

Vertical profiles of ice crystal size distributions in cirrus clouds were obtained for 37

cases observed by the HYVIS. Hereafter, the minimum and maximum altitudes where ice particles were detected are referred to as cloud base and cloud top, respectively. Therefore, ice saturation and/or supersaturation could not be assured inside the clouds presented here. Cloud depths (actual vertical distances) varied from 1.1 to 8.8 km (average: 4.8 km) with cloud top heights ranging from 8.2 to 14.1 km and base heights from 2.7 to 11.9 km. Cloud top temperatures ranged from −33° to −72°C, while base temperatures from −3° to −49°C.

The HYVIS data were averaged over every 250 m-thick sub-layers in each case. For each sub-layer, we calculated the ice water content (IWC) and cloud volume extinction coefficient (β_{ext}). The empirical power-law relationships between mass (m) and maximum dimension (D) and cross-sectional area (A) and D are used in summing up the values of all particles. The power-law equations of m-D and A-D relations used in this study are shown in Fig. 3.1, based on the results of Davis (1974), Heymsfield and Kajikawa (1987, hereafter HK87), and Mitchell et al. (1996). The β_{ext} is assumed to be twice the cross-sectional area of particles because the extinction efficiency is approximately 2. By using the HYVIS-measured size distribution, we can estimate the ice water path (IWP)and optical thickness τ_{hyvis} of the entire cloud layer from the integration between the cloud base and cloud top of the IWC and β_{ext}, respectively.

For the image processing of the HYVIS measurements, the particle size (maximum dimension), concentration, and crystal habit of cirrus cloud particles were derived from each image, which was manually determined and processed. Because the HYVIS images were recorded as a motion picture, separation of overlapping particles or determination of ice crystal breakup during impaction on the film by visual analysis is facilitated, which has been inferred from frame-by-frame analysis. The fragmentation by breakup upon impaction with the HYVIS was observed to be about 5% of the total counts at most in our dataset, and such particles were excluded in order to avoid any artificial concentrations.

Automatic image processing was also utilized to obtain the cross-sectional area (A), maximum dimension (D), major axis length (a), and minor axis length (b) of each particle in the microscopic camera images. The particles size ranged from about 10 to 200 μm. The particle images recorded by the close-up camera, however, were not processed because the image quality was inadequate for estimation of shape parameters.

In this study, we examined shape-sensitive parameters in terms of aspect ratio and area ratio (A_r). We defined the aspect ratio of each ice particle to be the axis ratio (= b/a), i.e., the ratio of the lengths of the minor and major axes. We defined A_r to be the ratio of A to the area of a circumscribed circle with a diameter equal to the maximum dimension of the particle, i.e., $A_r = A/(\pi D^2/4)$. Compact particles with nearly circular shapes have an A_r nearly 1.0, whereas elongated, flat, or stellar particles have a lower A_r.

3.2 Vertical profiles of thermodynamic data

Relative humidity (RH) and temperature profiles were simultaneously measured with a rawinsonde (JMA model RS2-91; Meisei Electric Co.) whose signals were transmitted on a 1673-MHz microwave carrier. Since the 2004 campaigns, a GPS sonde (Model RS-01G; Meisei Electric Co.) was used to measure meteorological parameters, whose humidity sensor has basically the same specification as that of the RS2-91 rawinsonde. The RH sensor uses the principle of a thin-film capacitive method; the same principle is used by the Vaisala RS80-A sensor. At cold temperatures, this type of RH sensor exhibits a dry-bias error that increases significantly with decreasing temperature below −30°C (Miloshevich et al. 2001). Because the magnitude of the measurement error depends highly on the type of sensor and a correction algorithm for our sensor is yet to be developed, we presented the uncorrected data of RH measurements in this study.

RH profiles are one of the crucial factors affecting the size distributions of ice crystals. Figure 3.2 shows the vertical distributions of the RH with respect to ice observed within

the cirrus clouds. Clearly, the RH rapidly decreased with decreasing height in the cloud regions, $NormH < 0.1$, although there would have been significant underestimation in the rawinsonde RH measurements at low temperatures.

The vertical profiles of thermodynamic stability might provide some indication of whether the cirrus crystals were produced in large-scale ascent, with vertical velocities of the order of 1–10 cm s^{-1}, or in smaller-scale convective cells with vertical velocities of the order of 100 cm s^{-1}, as shown in Fig. 3.3. Stability was examined by calculating the lapse rate (Γ_{PTE}) of equivalent potential temperature from every 8-s measurement of RH and temperature for each cloud sublayer including 100 m above and below a reported level of rawinsonde measurements. A neutral stability refers to the condition where Γ_{PTE} in the figure is near zero. The thermodynamic conditions in the upper half of the clouds tend to be neutral with respect to equivalent potential temperature, except the regions very near the cloud top. Meanwhile, the stability in the lower half of the clouds, except the cloud bottom regions, showed a discernible tendency to increase with decreasing height. This is determined primarily by the structure of a warm front. Sublimation and associated local cooling near the cloud base would have produced relatively large lapse rates near the cloud base.

3.3 Examples of cirrus clouds observations

The HYVIS is attached to a balloon with a rawinsonde and a radiation sonde (Asano et al. 1994) and they are launched into clouds. This combination provides us with vertical profiles of microphysical, thermodynamic, and radiative properties in cirrus clouds. The radiative properties of cirrus clouds observed by the radiation sonde were reported in Yoshida et al. (2004).

Two examples for the microphysical properties of cirrostratus clouds are shown in this section. Cirrostratus associated with a stationary (Baiu) front was observed over the

Tsukuba Area, Japan, on 8 June 1995. The balloon with the above combination was launched at 1030 and 1631 JST (hereafter all times are Japan Standard Time). Figure 3.4 shows profiles of temperature, relative humidity, and wind obtained from the 1030 sounding. On the observation day, the tropopause located at almost the same altitude as the cloud tops (~13.5 km) and a jet core was located about 200 km north of the observation site.

Figures 3.5 show the vertical distributions of ice crystal number concentrations, ice water contents, and extinction coefficients of clouds computed from particle images for the 1030 and 1631 cases, respectively. High concentrations of ice crystals were confined to the upper layer of about 300 m deep for the 1030 case, and to the upper layer of about 2 km deep for the 1631 case. Simultaneous radar observations on that day suggested that the HYVIS penetrated generating cells embedded in cirrostratus. In Fig. 3.5, the integrated values of IWP and τ_{hyvis} in each case are shown on top of the panel b and panel c, respectively.

Size distributions from close-up and microscopic images were combined at 250 m intervals and their vertical changes are shown in Fig. 3.6. Every size distribution could be fitted by a gamma distribution. The detailed analysis on size distributions observed by the HYVIS will be described in section 8. Major shapes of ice crystals observed in the clouds were bullets, columns, bullet rosettes, and combinations of columns and plates. A considerable number of plane-type crystals were also found in lower levels in each case. For both cases, high concentrations (more than 100 particles per liter) of ice crystals were found near the cloud tops. The main component of the crystals observed there was the bullet (and bullet rosette) of 100–250 μm in size for the 1030 case while it was nascent bullet rosette of about 50 μm for the 1631 case. Statistical analyses on number concentrations and shapes of ice crystals from the HYVIS dataset will be described in sections 4 and 6, respectively.

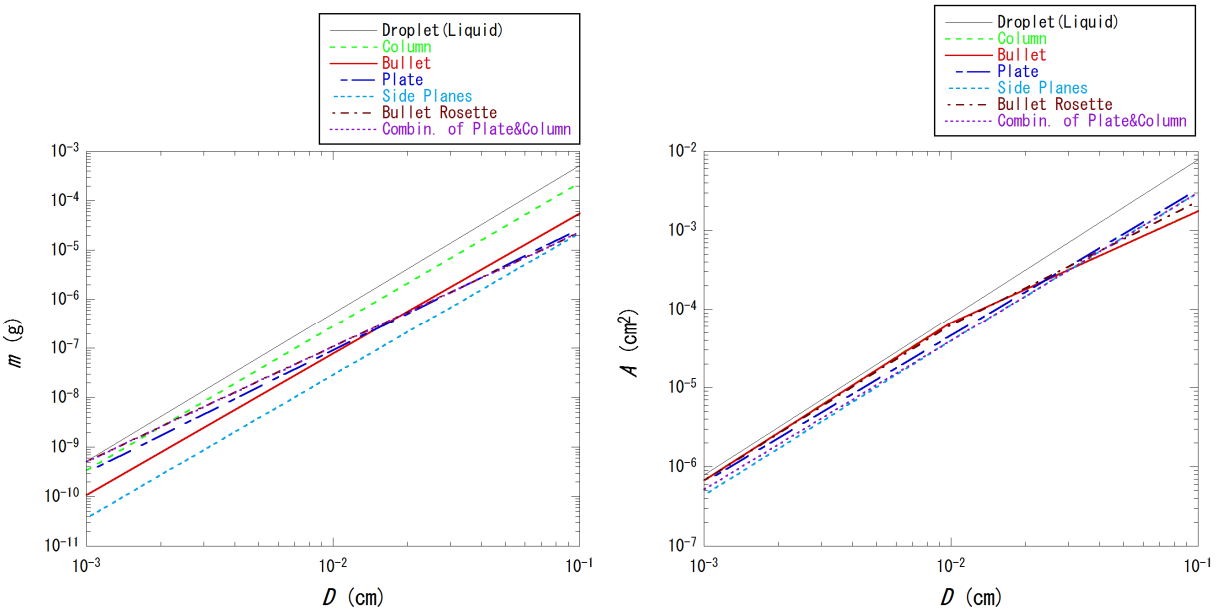

Fig 3.1 Relationships between mass (panel a) or cross-sectional area (panel b) and maximum dimension for various ice crystal habits. The black solid line indicates the curve for water droplet for reference.

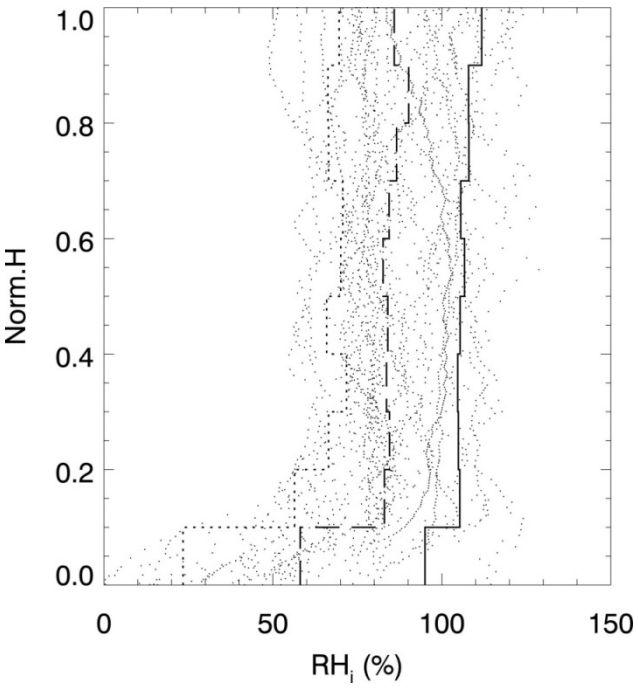

Fig 3.2 Profiles of relative humidity with respect to ice as a function of normalized height (*NormH*) within the cirrus clouds observed in this study. The dotted line, dashed line, and solid line indicate the 10th, 50th, and 90th percentiles, respectively.

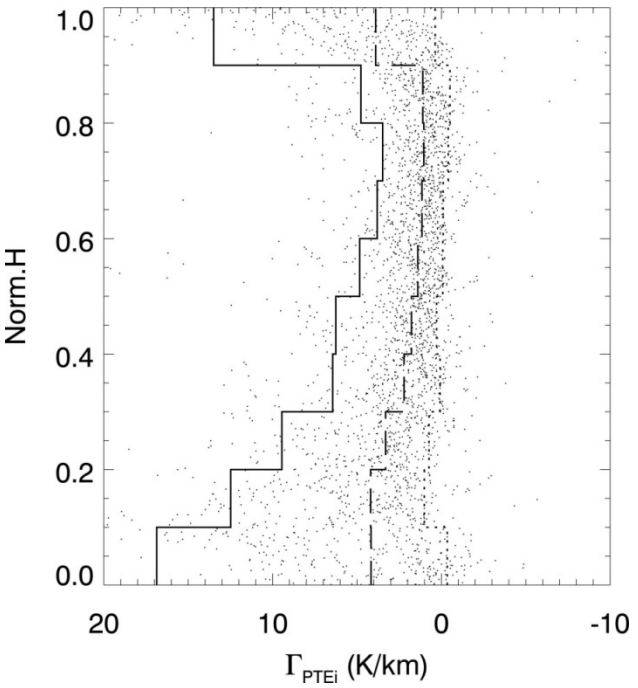

Fig 3.3 Same as Fig. 3.2 but for thermodynamic stability profiles. Each point was derived from the lapse rates of equivalent potential temperature in each cloud sublayer including 100 m above and below a reported level from rawinsonde measurements.

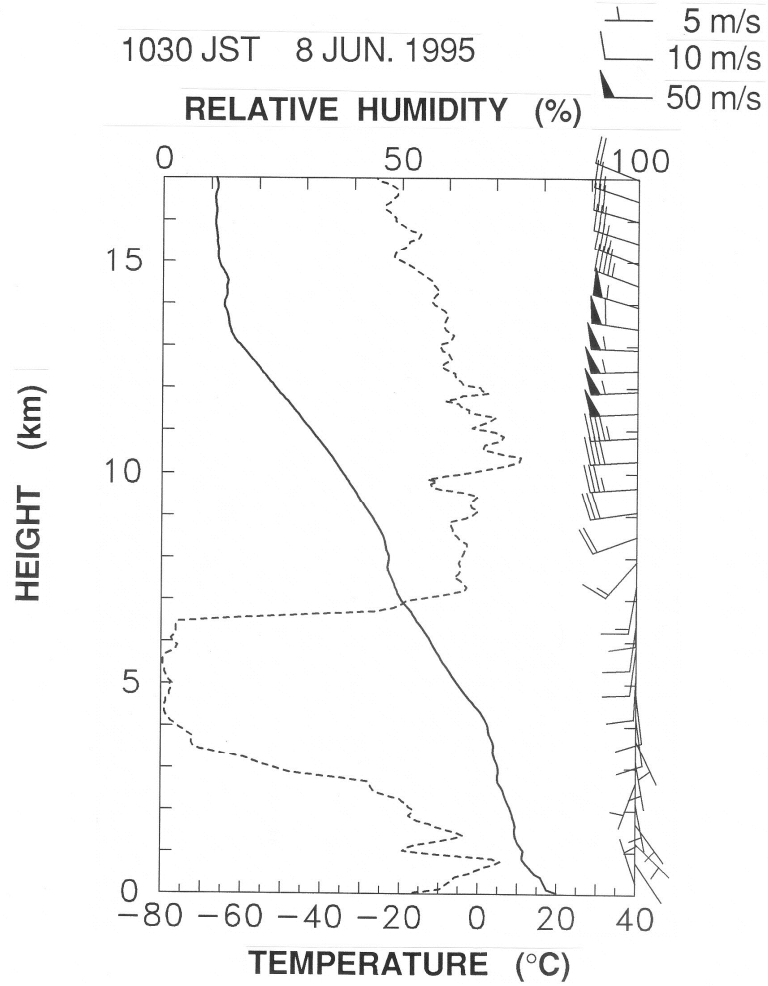

Fig 3.4 Vertical profiles of temperature (solid line), relative humidity (dashed line) and wind measured by a rawinsonde combined with the HYVIS launched at 1030 JST on 8 June 1995.

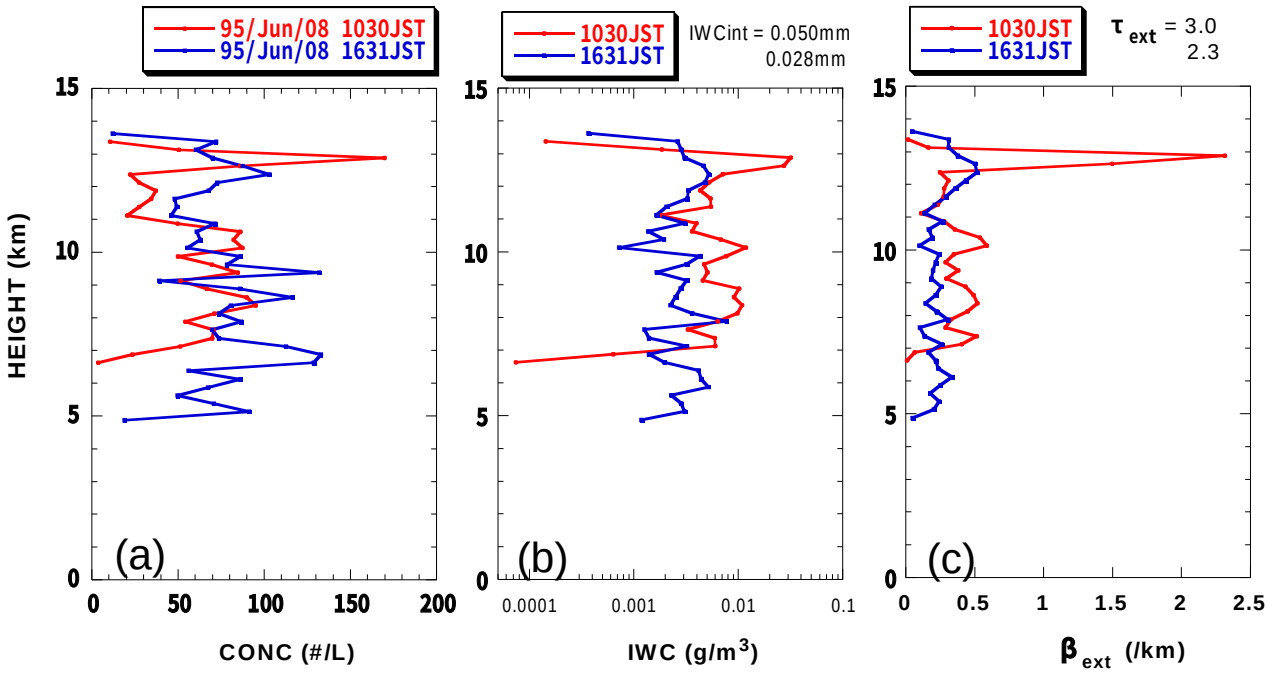

Fig 3.5 Vertical structures of the cirrostratus measured by the HYVIS launched at 1030 (red) and 1631 (blue) JST: (a) number concentration of ice crystals; (b) ice water content; (c) extinction coefficient of clouds.

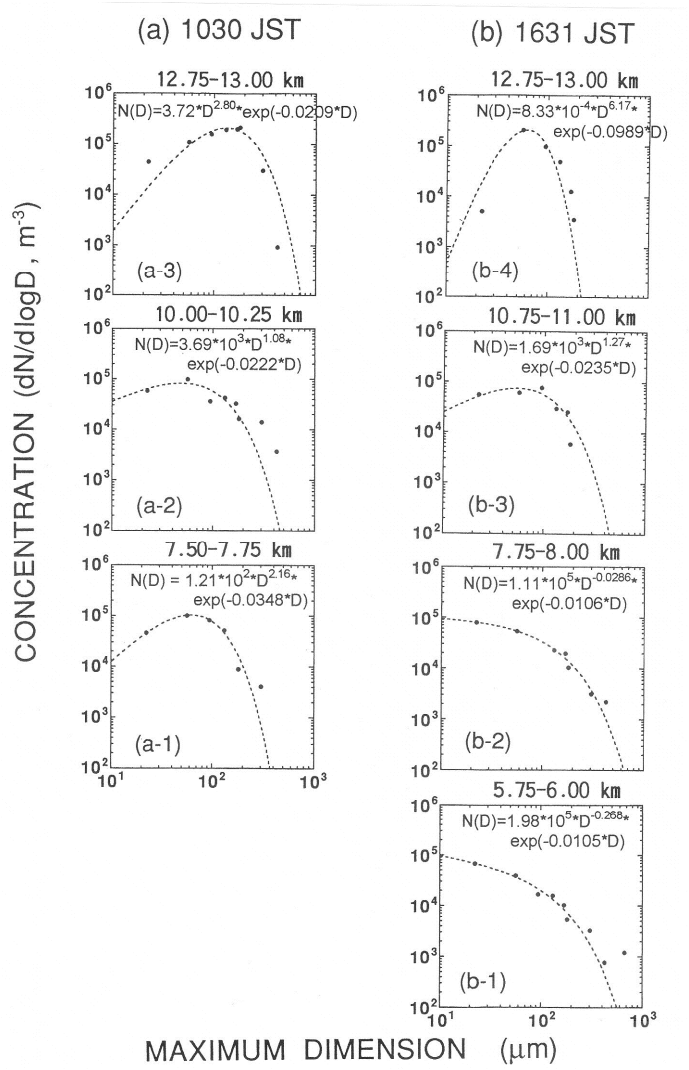

Fig 3.6 Change in size distributions of ice crystals along the ascent of the HYVIS: (a-1), (a-2) and (a-3) for the 1030 case; (b-1), (b-2), (b-3) and (b-4) for the 1631 case. Dashed lines in each panel are regression curves and their formulae are shown at the top of each panel.

4. Number concentrations of ice crystals in cirrus clouds

4.1 Results of ice crystal concentration data

Size distributions from close-up and microscopic images were combined at 250 m height intervals. Figure 4.1 shows examples of size distributions measured by the HYVIS. Only the size distributions near the cloud top are shown because most ice crystals in this region are likely to be nucleated in this region and less affected from other regions. For some distributions in Fig. 4.1, the concentration falls off rapidly for sizes smaller than 50 μm, while particles are fed into the smallest bin in most of the size distributions. The HYVIS measurements also show broad size distributions with gentle slopes, even at cold temperature (−50° to −70°C), where the growth rate of ice crystals is significantly lower than that at a warmer temperature (>−40°C) under the same ice supersaturation. The gentle slopes in smaller size ranges suggest that no intensive ice nucleation could occur. In such a case where tiny ice particles are dominant in the size range from a few microns to 10 μm, the HYVIS measurements show large errors in the total number concentrations. Although this is a limitation for the instrument, it is unlikely that the measured concentrations in the synoptically generated cirrus in our dataset would cause a systematic bias to the profiles of ice particle populations, which is inferred from the uncertainty of the *CE* of the HYVIS, the measured size distributions of ice particles, and the comparison between the measured and simulated number concentrations mentioned in section 4.2.2.

The results of vertical distributions of total ice crystal concentrations are shown in Fig. 4.2, where the ice crystal concentrations are plotted as a function of normalized height (*NormH*) such that cirrus cloud base height = 0 and cloud top height = 1 in a relative sense in each case. These plots are classified according to the cloud top temperatures, as shown. Although the dataset had fewer cases with cloud top temperatures above −55°C, ice crystal concentrations varied from the order 10^{-1} to 10^{2} L^{-1}. The concentrations of ice

crystals larger than 30 μm are also shown as the median value (dashed line) in Fig. 4.2. There was little difference between the two concentrations, including and excluding ice crystals in the size range of 10–30 μm.

The number concentrations of ice crystals were sometimes the highest near the cloud top; however, their trend of increasing with distance below the cloud top is shown in Fig. 4.2. In contrast, the ice crystal concentrations decreased in the vicinity of the cloud base owing to sublimation, although aggregation could occur for some of the clouds. To examine where the maximum ice crystal concentration occurred in the vertical distributions of the ice clouds, Fig. 4.3 shows both geometrical distances from the cloud top and cloud normalized heights where the maximum concentration occurred as a function of cloud depth. The maximum concentrations occurred at various heights inside cirrus clouds; about 35% of all cases had the maximum concentration near the cloud top ($NormH \geq 0.8$), 16% near the cloud base ($NormH < 0.2$), and 49% around the middle of clouds ($0.2 \leq NormH < 0.8$). There was no correlation between the cloud depth and normalized height or distance below the cloud top with the maximum concentrations. However, which stage of cloud evolution in cirrus clouds the HYVIS penetrated should be considered in order to further understand the vertical microphysical structure, which we were unable to determine owing to poor coordination with other observation devices in both time and vertical columns.

Ice crystal habits detected from the HYVIS imagery were examined to infer whether some of the enhanced concentrations near the cloud base or the sublimation zone ($NormH < 0.1$) as shown in Fig. 4.3 could have been due to the breakup of rosettes; Gow (1965) reports that single bullets result from the breakup of rosettes from sublimation. Ice crystals detected by the HYVIS measurements were classified visually according to their crystal habits. The single bullet type of ice crystals was dominant, as shown in Fig. 4.4. In this figure, the occurrence frequency of bullet rosettes decreased with decreasing height.

Also shown is the tendency toward an increase in the frequency of single bullet or column near the cloud base. These results together with the RH profiles are consistent with the scenario that single bullets are formed as a result of the breakup of bullet rosettes in sublimation regions (Gow 1965). The breakup of bullet rosettes may be attributed to one of the major factors that produced the maximum concentrations even near the cloud base. The laboratory study by Dong et al. (1994), where ice particle breakup during evaporation produced secondary ice crystals, could also support the breakup of bullet rosettes under subsaturated conditions in cirrus clouds.

To obtain smooth (or representative) size distributions of ice crystals, vertical averaging of the HYVIS data is usually taken over 250-m-thick cloud layers. To verify whether the vertical averaging affects the interpretations, we test several ways of averaging. The vertical profile of the measured ice crystal concentrations can be resolved into fine intervals (~10 s) on the basis of the analysis of each video image, which corresponds to a vertical resolution of 40–140 m (average: 80 m), according to ascent rates (typically 6–8 m s^{-1}) of the HYVIS. (It takes about 5–15 min to penetrate a vertical column of cirrus.) Figure 4.5 provides the comparison of the maximum ice crystal concentrations with degraded vertical resolutions (250 m, 500 m, and 1 km); it displays distributions of the maximum concentration in the whole cloud region and four cloud regions partitioned by normalized height. The degradation of vertical resolution had a major impact on finding high concentrations in every case because its statistics consistently decreased with increasing vertical intervals and had no discernable effect on the concentrations among different vertical relative locations. It was shown in Fig. 4.5 that the vertical averaging over 250 m can be deemed acceptable to discuss the range of ice crystal concentrations in the vertical.

4.2 Discussion and implications of the measured concentrations

In this section, we first present the cirrus microphysical measurements from the other balloonborne ice crystal collector, the ice crystal replicator (Miloshevich and Heymsfield 1997), in order to obtain further support for the number concentrations measured by the HYVIS presented in section 4.1. Second, by comparing the HYVIS measurements and the recent results of cirrus modeling studies, some implications for ice nucleation mechanisms in cirrus clouds are discussed.

4.2.1 Comparison with ice crystal replicator data

The microphysical data of the balloonborne ice crystal replicator presented here were collected on November 25, November 26, and December 5 in 1991 during the FIRE II experiment near Coffeyville, Kansas (Miloshevich and Heymsfield 1997). These data and the associated ice particle imagery have been reported in Miloshevich and Heymsfield (1997). These three cases had cloud top temperatures (altitude) of −56.9° (10.41 km), −53.3° (9.74 km), and −65.4°C (12.63 km), respectively.

Similar to Fig. 4.2, for the HYVIS measurements, the vertical distribution of ice crystal concentrations are shown in Fig. 4.6. Although there were limited cases with replicator data, the ice crystal concentrations ranged from the order 10^0 to 10^2 L^{-1}, which is similar to the results of the HYVIS measurements. The vertical distributions exhibited the highest ice crystal concentration in the middle of the cloud or near the cloud top and typically low concentration in the lower half of the cloud.

4.2.2 Implications of ice crystal concentrations from HYVIS measurements

In the Cirrus Parcel Model Comparison (CPMC) Project (Lin et al. 2002), under the GEWEX Cloud System Study (GCSS) Working Group on Cirrus Cloud Systems (WG2), systematic efforts were directed toward assessing the understanding of ice crystal nucleation and evolution of microphysics in a closed air parcel by comparing with cirrus

simulations using seven models. Although qualitative agreement has been found among the models for the simulations only with homogeneous nucleation, significant differences were reported in the comparison of predicted ice crystal concentrations. Lin et al. (2002) reported that some critical factors affected the predicted concentration, such as homogeneous ice nucleation rate, haze particle solution concentration, and growth rate of small ice crystals.

Ongoing laboratory studies in conjunction with modeling studies are becoming an important approach to improve our understanding of cirrus ice formation mechanisms (DeMott 2002, 2007). The laboratory results are useful for formulating the cirrus cloud processes in numerical models where many aspects are poorly understood and are not well-incorporated. To explore the relevance of ice crystal nucleation events in cirrus, we make qualitative comparisons between the HYVIS observations and previous cirrus modeling studies focused on homogeneous and heterogeneous ice nucleation. In the HYVIS dataset, we had no information of primary importance to ice crystal nucleation, including the updraft velocity and size spectra and chemical composition of both CCN and IN. Accordingly, our intention is to examine the range of possibilities on the ice nucleation process. For quantitative comparisons, such additional information from observations is required at the minimum to simulate cirrus formation, which is beyond the scope of this study.

As an example of the simulation of homogenous ice nucleation, we perform sensitivity tests in this study by using the parcel model of Heymsfield and Miloshevich (1993). Although their model was not included in the study by Lin et al., the predicted ice crystal concentration was within the limits of differences among the seven models. The Lagrangian parcel model was run in a closed air parcel with prescribed, fixed updrafts, where no particle fallout was allowed (details in Heymsfield and Sabin 1989). Constant updraft velocities of 10, 50, and 100 cm s^{-1} were used here as a sensitivity test for these

simulations. The initial atmospheric environment (temperature, relative humidity, and pressure) was set on the basis of standard atmosphere with subsaturated conditions with respect to water: 90% at −40°C, 70% at −60°C, and linearly interpolated relative humidities at temperatures between the two abovementioned temperatures. Although the physical and chemical properties of aqueous aerosols are fundamental information for homogeneous ice nucleation, the aerosol with one composition namely ammonium sulfate CCN was assumed, whose supersaturation spectrum was given by the power-law form ($N_{CCN} = CS^k$, where N_{CCN} (cm^{-3}) is the total CCN concentration that is activated when a supersaturation with respect to water S (%) is achieved) with constants C (scaling factor, cm^{-3}) and k (slope) of 100 and 0.5, respectively, and coincident observations of CCN narrow the uncertainties associated with this aspect. (Sensitivity tests on the CCN spectrum were given in Heymsfield and Miloshevich (1995); ice crystal concentrations can be substantially reduced if a limited number of effective CCN are available for homogeneous ice nucleation.) As pointed out by Lin et al. (2002), the deposition coefficient given in the modified vapor diffusion coefficient follows the findings of Fukuta and Walter (1970), which affects the growth rate of small ice crystals (<10 μm), and vapor depletion rate has a substantial impact on the resulting ice crystal concentration. Here we assumed 0.04 as the typical value of the deposition coefficient. Increasing this parameter to unity results in a decrease of ~1 order of magnitude in the predicted concentration. Although the deposition coefficient is still an unknown parameter that may depend on environment variables such as temperature and supersaturation as well as size and surface structure of individual particles, the result of a recent laboratory experiment (Magee et al. 2006) supports the hypothesis of the numerical modeling study by Gierens et al. (2003) that the deposition coefficient is significantly smaller than unity, 0.01 or less in low-temperature conditions (<−40°C) with weak updrafts relevant to typical cirrus clouds.

Figure 4.7 shows the ice crystal concentrations measured with the HYVIS as a

function of local temperature in clouds in comparison to the abovementioned homogeneous ice nucleation simulation. The Fletcher's (1962) ice-nucleus curve and the parameterization by Meyers et al. (1992) for contact freezing and deposition/condensation freezing are also shown for reference. In Fig. 4.7a, the HYVIS data from all cirrus measurements are shown; concentrations are partitioned into the 10th, 50th, and 90th percentiles. In Figs. 4.7b–d, the data are plotted for the lower 20% of the cloud (panel b), middle of the cloud (20% to 80% of the normalized height; panel c), and upper 20% of the cloud (panel d).

The measured ice crystal concentrations exhibited values over a wide range from the order of 10^{-1} to 10^{2} L^{-1}. Although it becomes critical to verify whether the simulation describes the conditions under which the HYVIS observations were made, there was a large difference between the measured concentrations and the calculated ones, even if we might expect slow updrafts (~10 cm s^{-1}) in cirrus formation. Furthermore, the observations did not indicate a temperature dependence derived for the simulations.

However, one might expect that other physical processes besides the ice nucleation process could predominantly result in a weak temperature dependence of the ice crystal concentrations. In general, it is difficult to separate the effect of each process on ice crystal concentrations. A complete discussion of these interpretations is beyond the scope of this study.

The comparison in Fig. 4.7 should be appropriate if small ice crystals are assumed to be nucleated in the vicinity of the measured levels and to dominate the total concentration. To complement the result shown in Fig. 4.7, Fig. 4.8 shows the relationship between cloud top temperature and maximum ice crystal concentration in each case of the HYVIS dataset. Similar to Fig. 4.7, no obvious dependence of the measured ice crystal concentrations on temperature was found. Instead of the homogeneous-only ice nucleation simulation, the simulations that focused on the combination of the

homogeneous and heterogeneous ice nucleation were qualitatively compared with the HYVIS observations, as shown in Fig. 4.8, although our poor understanding of heterogeneous ice nucleation mechanisms could result in wide ranges in the predicted concentrations. We cite studies by Jensen and Toon (1997) and DeMott et al. (1997) on the parcel model simulations involving both ice nucleation mechanisms. Jensen and Toon (1997) used a classical model of a spherical ice cap on the insoluble particle whose efficiency as heterogeneous freezing nuclei was given by the contact angle parameter ($m_{i/n}$). Although they assumed that $m_{i/n} = 0.8$, the results might include the uncertainties caused by very poor freezing nuclei ($m_{i/n} < 0.3$). On the basis of the results of parcel model simulations by Jensen and Toon (1997), only the case of moderate number density (0.1 cm^{-3}) of soot particles acting as freezing nuclei was referred here for comparison because it could be regarded as the background value in the upper troposphere. DeMott et al. (1997) used an empirical approach defined as the effective freezing temperature (T^*). This parameter was proposed by Sassen and Dodd (1988), and in this definition ($T^* = T + \lambda \delta T_m$), the empirical coefficient (λ) indicates the proportional constant for each individual solution between the freezing and equilibrium melting point depressions ($T^* - T$, δT_m, respectively). Although no available information is relevant to CCN and IN properties in our study, we referred to the results of only the simulation assuming sulfuric acid ($\lambda = 1$) as the CCN composition and unity as the number fraction of the CCN containing an insoluble component (corresponding to 10% of particle mass) given by DeMott et al. (1997). The latter assumption yields the maximum effect from heterogeneous freezing nucleation. A similar result of the predicted ice crystal concentration was reported when the CCN composition was ammonium sulfate ($\lambda = 1.7$), although their simulations suggested that the onset RH required for ice formation was significantly higher for the simulation assuming ammonium sulfate.

Although additional measurements are required to make definitive statements about

ice crystal concentrations and ice nucleation processes in cirrus clouds, the qualitative comparisons shown in Figs. 4.7 and 4.8 suggest the following:

● Peak ice crystal concentrations from the homogeneous-only nucleation simulation increased steadily from −40° to −60°C. In contrast, there was no discernable increase in the concentrations with decreasing temperature, even near the cloud top where most ice crystals were likely to be nucleated at adjacent heights and less affected through different heights (compared to other locations) by other microphysical and dynamical processes; concentrations were either flat or lower with decreasing temperature.

● The HYVIS measurements appeared to be closer to the lower concentration involving the heterogeneous nucleation simulations for the same magnitude of updraft velocity. As indicated by the homogeneous and heterogeneous nucleation simulation via the Jensen et al. scheme, the predicted concentration had a weaker dependence on temperature for the simulation with weaker updraft velocity (10 cm s^{-1}), which agrees better with the measured temperature dependence.

The above statements on implications of the HYVIS measurements are applicable even to mineral dust, which is one of the most dominant natural compositions among different types of aerosols for heterogeneous ice nucleation. Eidhammer et al. (2009) conducted an intercomparison of three different heterogeneous ice nucleation parameterizations proposed by previous studies focusing on the immersion or condensation freezing modes. Figures 3 and 4 in their study show the dependence of ice crystal concentrations predicted by the parcel model on vertical velocity and initial dust number concentrations. The initial temperatures (pressures) were −14° (800 hPa) and −40°C (340 hPa), respectively, and the details on the parcel model simulations were described in their paper. Even in regions of high dust concentrations (where heterogeneous ice nucleation is dominant), the three parameterizations differ in the predicted ice crystal concentrations by a factor of about 2 to 10 in the vertical velocity

range below 50 cm s^{-1} owing to freezing onset conditions and rates. However, within the same parameterization, the dependence of ice crystal concentrations on temperature or vertical velocity in case of dust particles is deemed to involve the same qualitative feature as the other cases in Fig. 4.8. The HYVIS measurements tend to be closer to the lower predicted concentrations of ice crystals in the heterogeneous nucleation regime, although the dependence on initial dust concentrations differs significantly among the three parameterizations.

As noted in section 2, the HYVIS measurements enabled us to acquire reliable size distributions of ice crystals above 30 μm or perhaps even smaller. Because we conclude that the measurements presented herein, although less accurate, do not substantially underestimate the total concentration in the observed cirrus clouds even when adding our 10–30 μm concentrations, we infer that the heterogeneous ice nucleation process is important (or even dominates) for the type of cirrus studied here, namely synoptically-generated cirrus. Research will be needed to further investigate the details of the relationship between the ice crystal concentration and ice nucleation processes active in cirrus clouds.

To infer whether our data suggest that heterogeneous ice nucleation is the dominant process, other recent field observations could be used to support our results. DeMott et al. (2010) showed that their measured IN number concentrations from nine field programs had a remarkable correlation with those of aerosol particles larger than 0.5 μm. In the mentioned study, the observed range of IN concentrations was restricted to temperatures above −35°C, where homogenous nucleation (freezing) does not occur. The similarity between these concentrations and our results suggest that the ice crystals in our study were predominantly formed by heterogeneous nucleation. We cannot rule out the possibility that within cirrus clouds or in cirrus forming regions, there are localized regions where homogeneous ice nucleation occurs sporadically; when this occurs, relative

humidities drop rapidly to prevent further homogeneous nucleation.

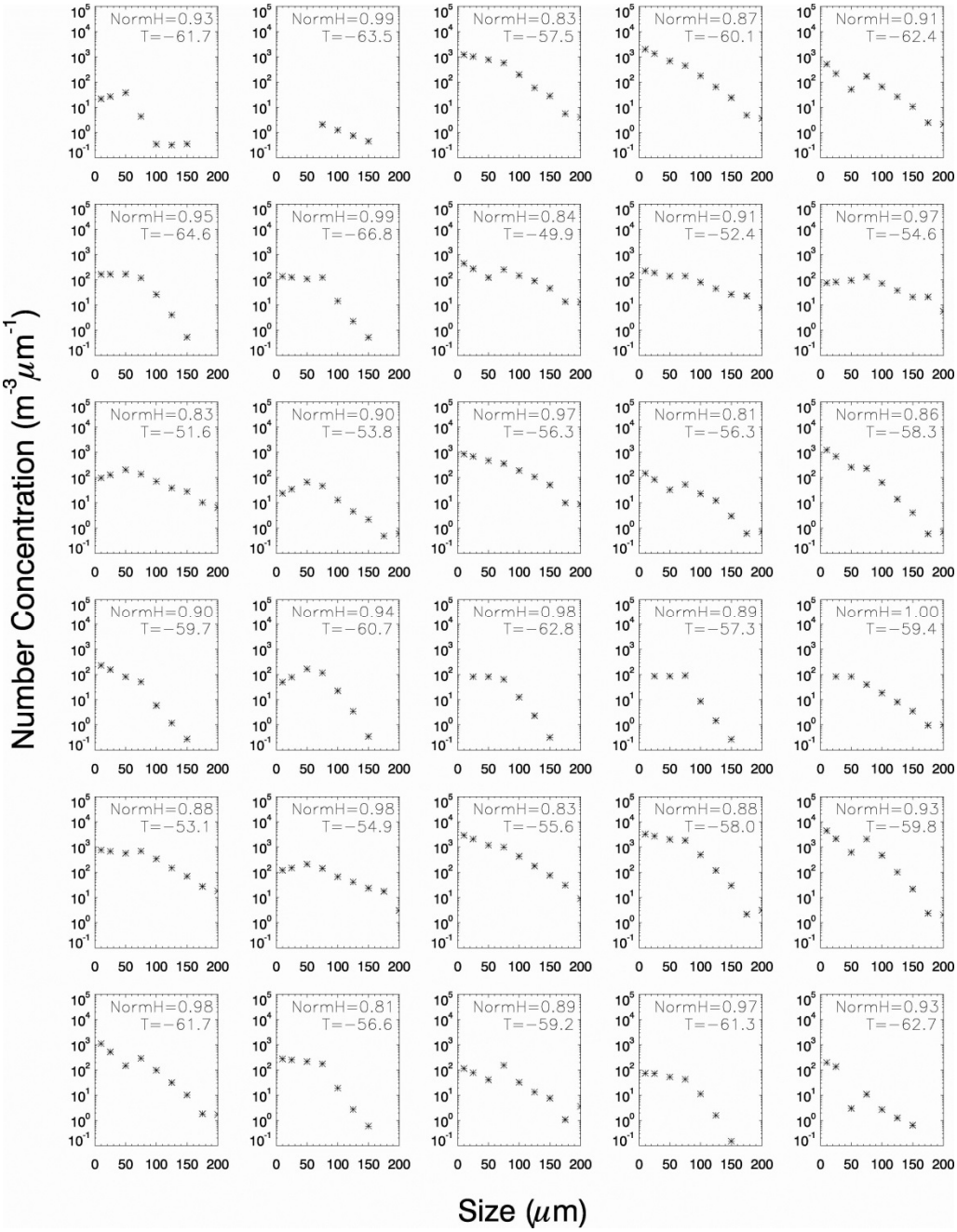

Fig 4.1 Size spectra up to 200 μm from HYVIS measurements in cloud top regions (*NormH* > 0.8). Normalized height and ambient temperature (°C) in upper right corner of each panel. Each panel represents a size spectrum averaged over a 250-m height interval.

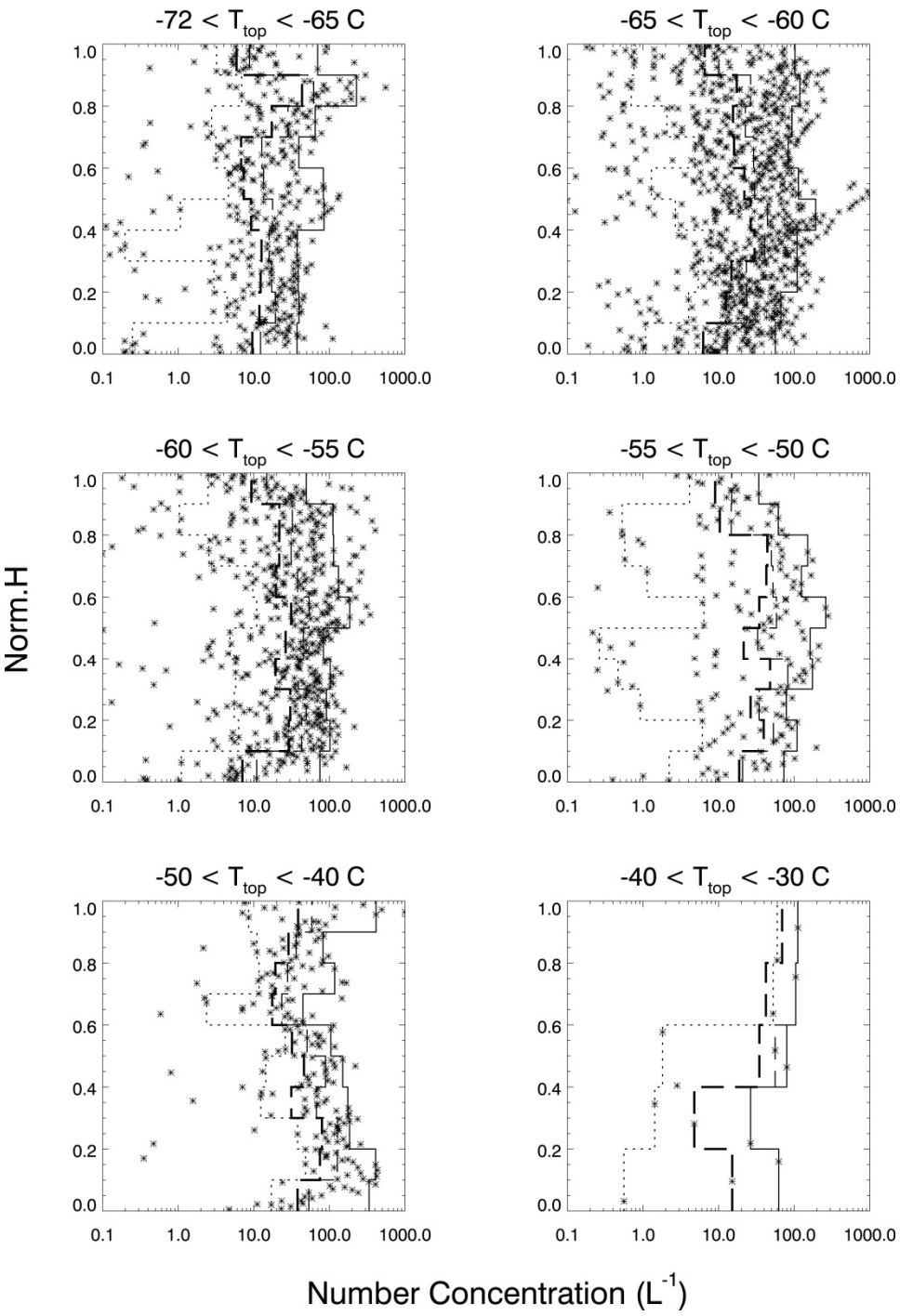

Fig 4.2 Vertical distributions of ice crystal concentration observed in this study as a function of normalized height (*NormH*), sorted by cloud top temperature; asterisk indicates each measurement of the HYVIS. In each panel, the dotted line, thin dashed line, and solid line indicate the 10th, 50th, and 90th percentiles of concentrations of particles larger than 10 μm, respectively, whereas the thick dashed line indicates the 50th percentile of concentrations of particles larger than 30 μm.

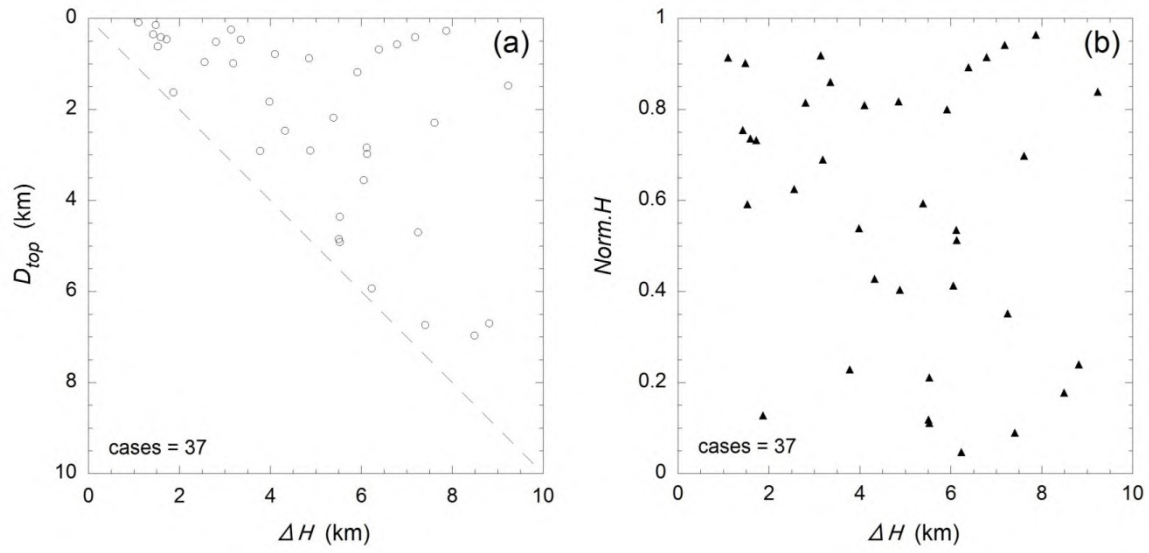

Fig 4.3 Geometrical distance from the cloud top (D_{top}: open circles, panel a) and normalized height (*NormH*: filled triangles, panel b) in each case where the maximum ice crystal concentration occurred as a function of cloud depth (ΔH). Dashed line in the panel (a) corresponds to cloud base ($\Delta H = D_{top}$).

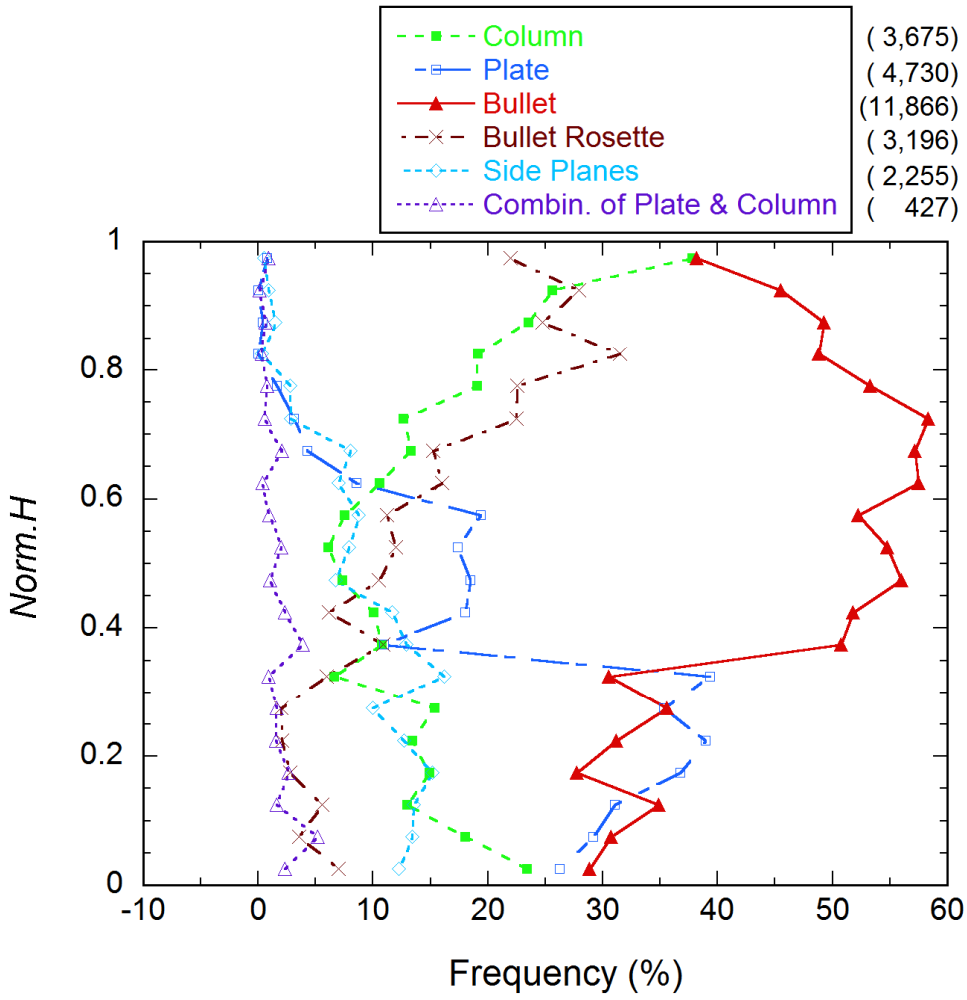

Fig 4.4 Average appearance frequencies of ice crystal habits as a function of *NormH*. The number next to the legend represents the total count of ice crystals in each category analyzed from the high-magnification (microscopic) images in the HYVIS dataset.

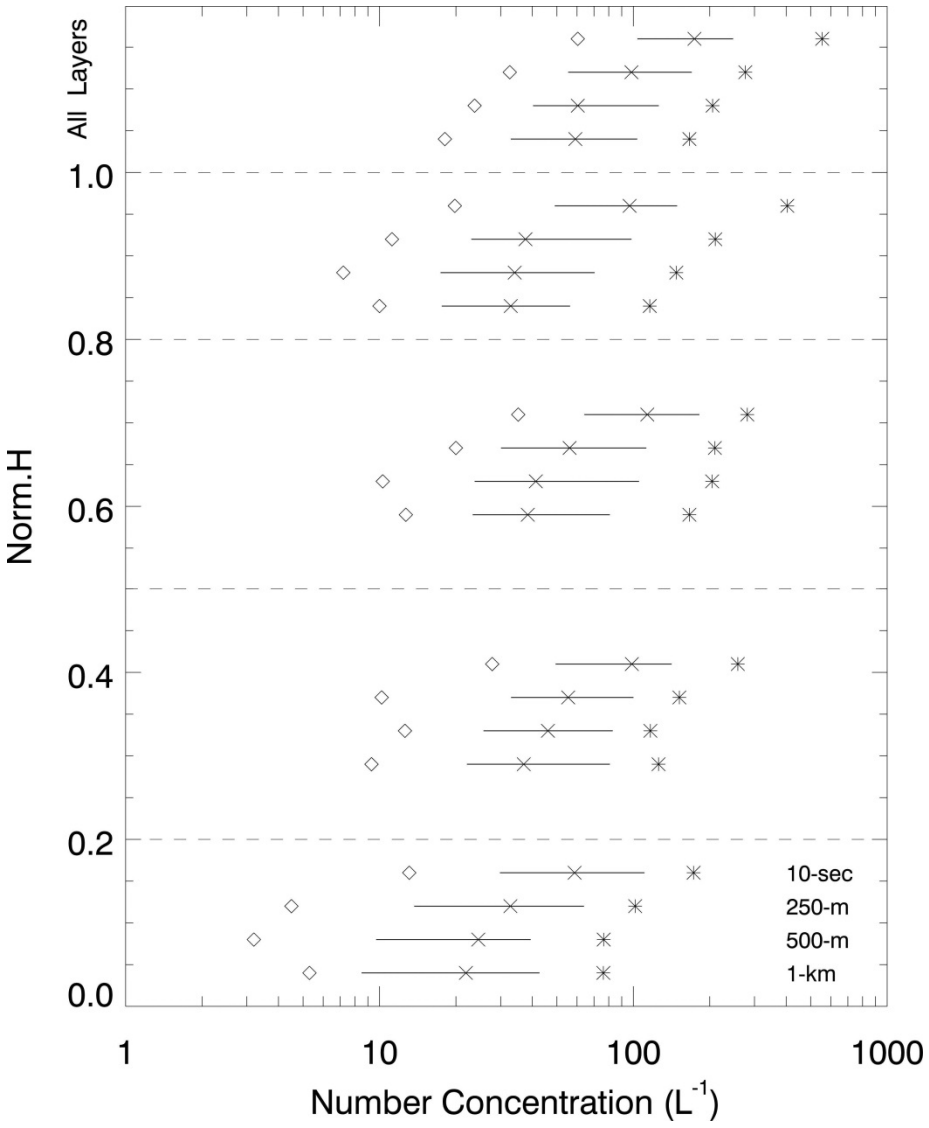

Fig 4.5 Comparison of distributions of the maximum ice crystal concentrations measured with the HYVIS for different vertical resolutions. The whole cloud layer is partitioned into four cloud regions according to normalized height, as indicated by horizontal dashed lines. The distributions of the maximum concentration in terms of the whole layer are also shown at the top of the figure. The four distributions shown in each domain of the figure are for 10-s (average: 80 m), 250-m, 500-m, and 1-km vertical resolution in order from the top, respectively. Solid lines represent the run between the 25th and 75th percentiles of number distributions. Diamonds, crosses, and asterisks represent the 10th, 50th, and 90th percentiles, respectively.

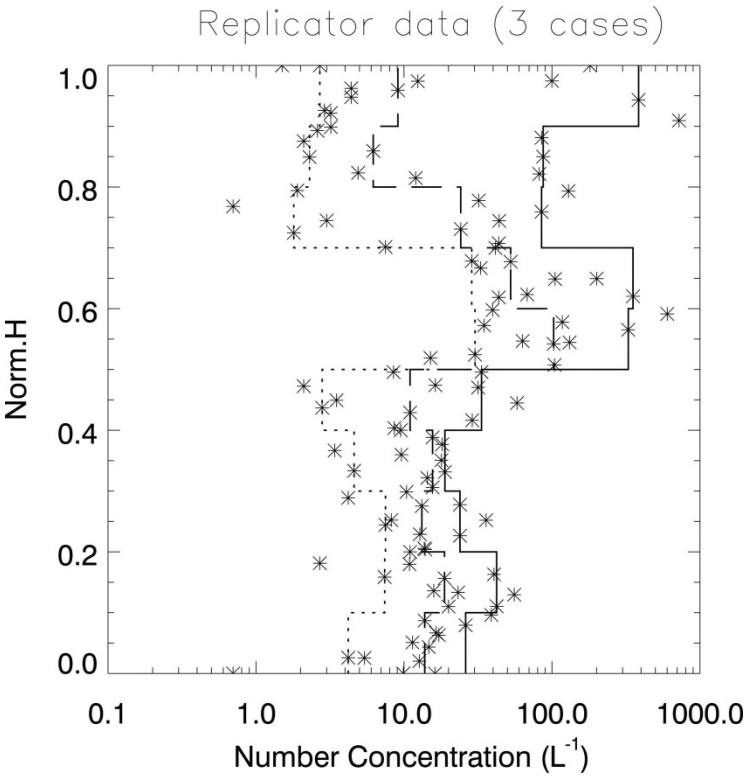

Fig 4.6 Same as Fig. 4.2 but for the ice crystal concentrations from the balloonborne ice crystal replicator data during the FIRE II experiment (courtesy of Larry Miloshevich).

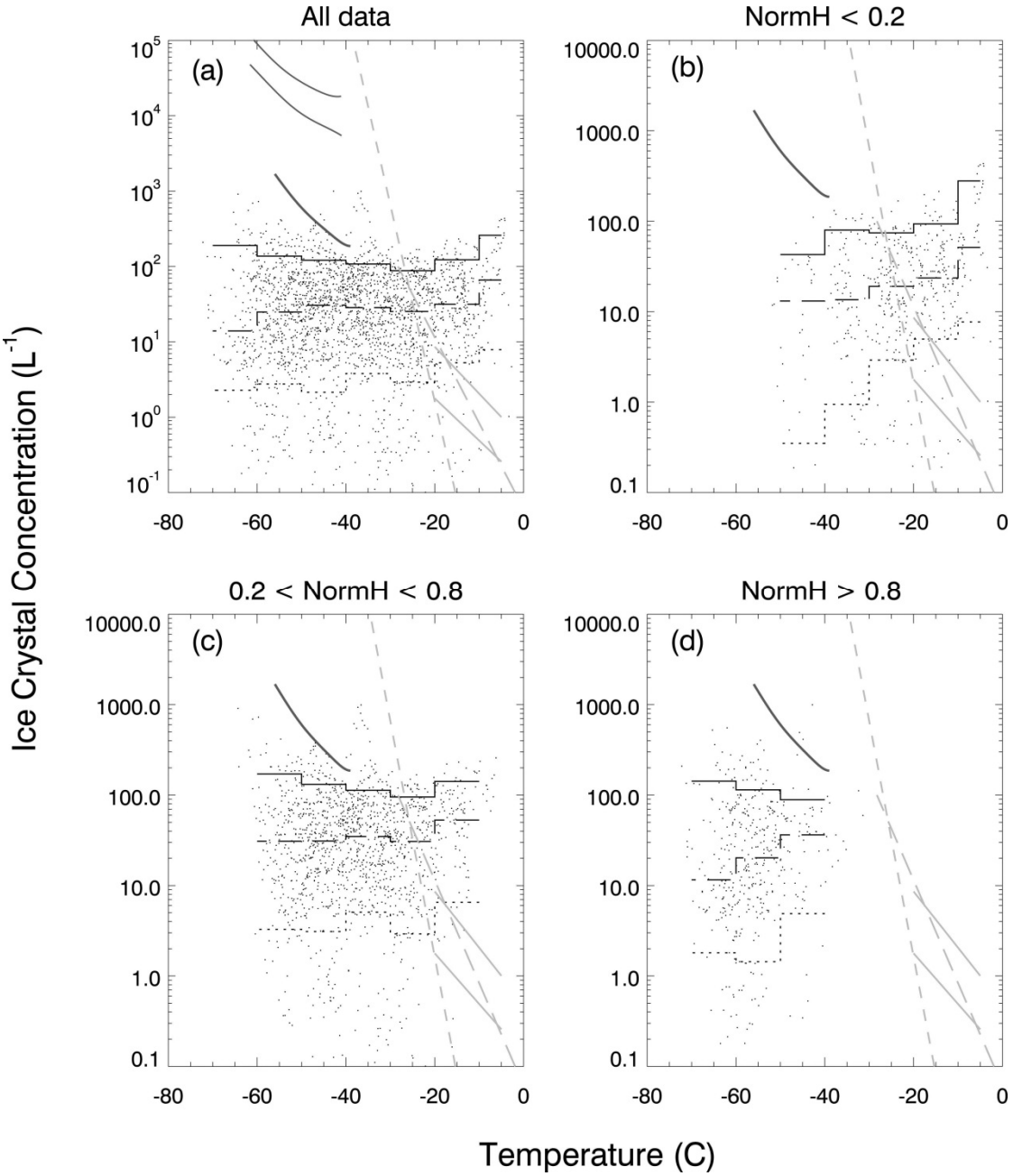

Fig 4.7 Comparison between ice crystal concentrations from HYVIS observations and simulated ones from parcel cloud modeling by Heymsfield and Miloshevich (1993) as a function of in-cloud local temperature. The HYVIS data are classified according to *NormH*: (a) all data; (b) *NormH* < 0.2; (c) 0.2 < *NormH* < 0.8; (d) *NormH* > 0.8. Horizontal stepwise lines indicate the 10th (dotted), 50th (dashed), and 90th (solid) percentiles of the HYVIS measurements in order from the bottom. Three regression black curves in Fig. 4.7a indicate the simulated maximum concentrations of ice crystals through homogeneous ice nucleation as a function of initial parcel temperature using three different constant updraft velocities (100, 50 and 10 cm s^{-1} from top to bottom in this panel), while only one case is indicated for the velocity of 10 cm s^{-1} in the upper left of Figs. 4.7b–d. Fletcher's ice-nucleus curve (thick gray short dashed line) and Meyers' parameterizations of both contact-freezing (thick gray long dashed line) and deposition/condensation-freezing (two thick gray solid lines: 0% and −10% supersaturation with respect to water in order from the upper) are also shown in each panel for reference.

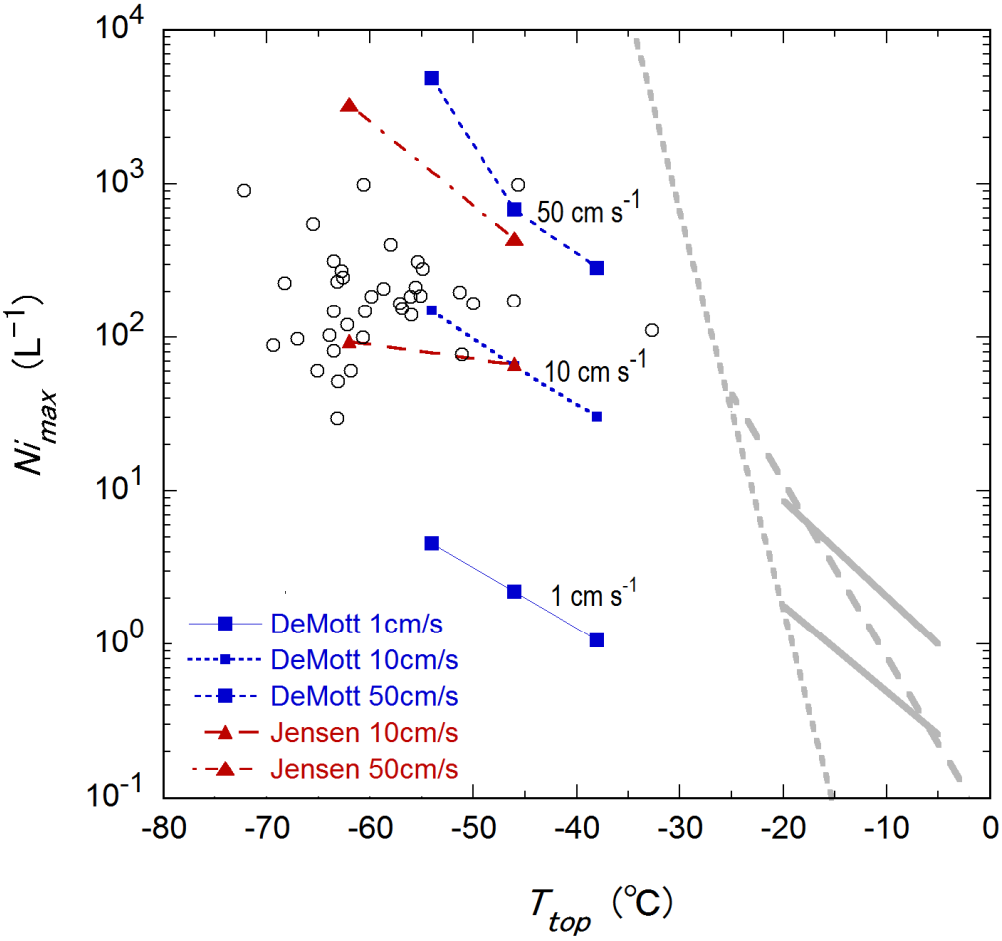

Fig 4.8 Maximum ice crystal concentrations (circle) from the HYVIS measurements as a function of cloud top temperature. The square and triangle markers indicate the simulated maximum concentrations of ice crystals, cited from DeMott et al. (1997) and Jensen et al. (1997) study, respectively, through both homogeneous and heterogeneous nucleation processes as a function of updraft speed and initial parcel temperature; details are given in the text. Three constant updraft velocities of 1, 10 and 50 cm s^{-1} are denoted by different marker sizes and line types as in the legend, except for the case of 1 cm s^{-1} in the simulation by Jensen et al., and the lines between the markers are logarithmic interpolations. Other thick gray lines are also shown for reference in the same way as that shown in Fig. 4.7, which indicate both Fletcher's ice-nucleus curve and Meyers' parameterizations.

5. Contributions of small ice crystals in microphysical and radiative properties

Small ice crystals (the maximum dimension $D < 100$ μm) can sometimes contribute to the most of microphysical and radiative properties in cirrus clouds. However, this is still uncertain due to limited observations of in situ data and difficulties of microphysical instruments to reliably measure small particles.

From our dataset observed in midlatitude cirrus clouds, we examine the contributions of small ice crystals measured with the HYVIS to the bulk parameters in terms of microphysical and radiative properties. Cirrus bulk properties such as projected area (A_c) and ice water content (IWC) are computed using the size distributions of ice particles and the contributions in each size ranges to the total are separately calculated for every 250m-thick layer of ice clouds.

Figure 5.1 shows the averaged contributions of ice crystals in each six size ranges to the total number concentration (NC) (panel a), A_c (panel b), and IWC (panel c). As for the NC, the contribution in size range of $D < 50$ μm was the most to the total for NC larger than 1 L^{-1}, while the contributions in size ranges of $50 < D < 100$ μm and $100 < D < 200$ μm became dominant for smaller A_c. As for the A_c, the contribution in size of $D < 50$ μm tended to decrease as the total A_c became larger, while the contributions in size ranges of $D > 100$ μm tended to increase. This tendency was similar to the IWC. The contribution to the total in size range of $100 < D < 200$ μm became most dominant for A_c larger than 0.05 mm^2/L and for IWC larger than 0.0005 g/m^3.

Figure 5.2 shows the averaged contributions of ice crystals in each six size ranges to the total as in Fig. 5.1, but for plotting against different sub-layers of ice clouds. Each cloud layer was divided into five equal-thickness between cloud top and cloud base for individual cases. On average, the contribution in size range of $D < 50$ μm was dominant for all sub-layers to the total NC, and the contribution in size range of $100 < D < 200$ μm was dominant to the total Ac and IWC except for the top sub-layer, where the

contribution in $50 < D < 100$ μm became most dominant.

McFarquhar et al. (2007) reported observations of tropical anvil cirrus during TWP-ICE campaigns, where small ice crystals with $3 < D < 50$ μm contributed 63%, 32%, and 20% to the total NC, A_c, and IWC on average when using CDP and CIP size distributions. This estimate was considered as being less affected by the instrument artifact of shattering of ice crystals occurring on the probe inlet. In the HYVIS dataset, the averaged contributions of ice crystals with $10 < D < 50$ μm to the total NC, A_c, and IWC were 53%, 19%, and 13%, respectively. These statistics showed about 10% smaller contributions of small ice crystals to the total, compared to tropical anvil cases. However, more data obtained on a global scale is required in order to extract a general conclusion.

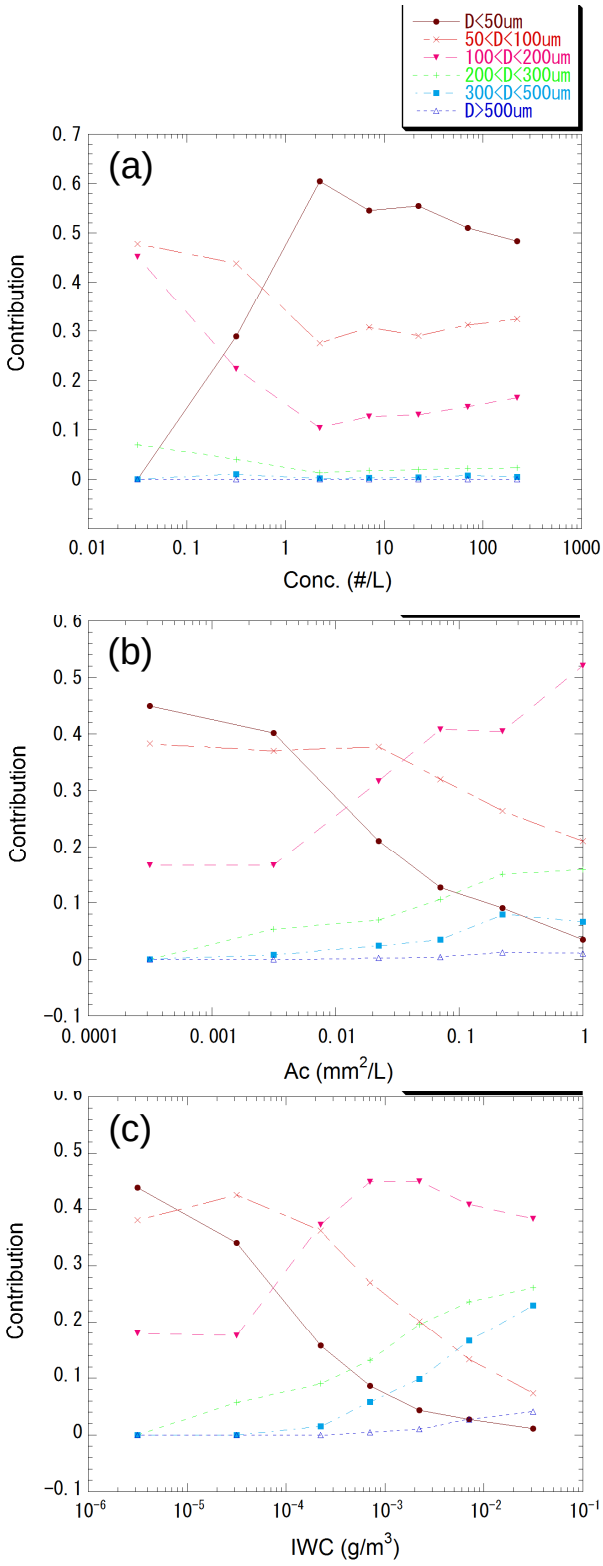

Fig 5.1 Averaged contributions of ice crystals in different size ranges to the total of (a) number concentration, (b) cross-sectional area, or (c) ice water content for every 250m-thick cloud layers.

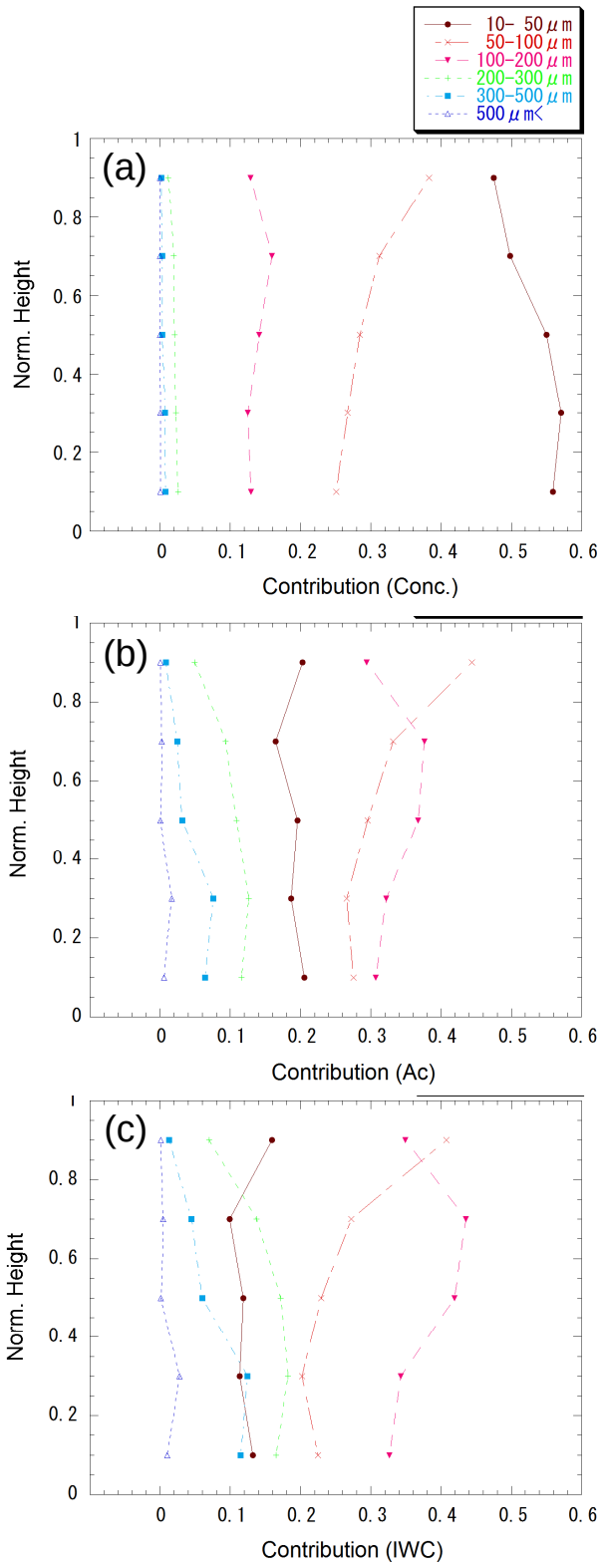

Fig 5.2 Same as Fig. 5.1 but for plotting against each five sub-layer normalized by the cloud thickness in each ice cloud case.

6. Ice crystal habits

6.1 Crystal habit frequency

In this study, the cirrus particle images measured with the HYVIS were classified into six major habit categories according to Magono and Lee (1966): column, bullet, plate, side planes, bullet rosette, and combinations (or aggregations) of columns and plates. A great majority (> 80%) of ice crystals smaller than 50 μm was unclassified owing to shape recognition being less reliable and the ice crystals being frequently quasi-spherical in shape; whereas over 80% of ice crystals larger than 100 μm were classified. In this study, the unclassified type is not included in the statistics of the ice crystal habits, as noted below. Examples of microscopic images in cirrus clouds obtained with the HYVIS are shown in Fig. 6.1; each classified type of ice crystals is accompanied with unclassified ice particles.

Figure 6.2 shows the frequency of the occurrence of ice crystal habits as a function of ambient temperature. It is apparent from Fig. 6.2 that the most prevalent habit was a single bullet crystal at temperatures ranging from –60° to –20°C. At temperatures between –60° and –35°C, the single bullet type was the most prevalent crystal type in the whole dataset (Fig. 6.2b). The plate type was dominant at temperatures warmer than –20°C, whereas the column or bullet rosette type became dominant at temperatures colder than –60°C (Fig. 6.2a). At temperatures colder than –40°C, the frequency of the bullet rosette and column crystals had a significant tendency to increase with decreasing temperature. At temperatures warmer than –40°C, the plate type had a discernible tendency to increase with increasing temperature. Side planes were more frequent at temperatures ranging from –45° to –25°C compared with other temperatures. The fact that there was a transition in the habit distribution observed in this study at a temperature of about –40°C is consistent with a recent laboratory study in which measurements were made with a static diffusion chamber (BH04).

The percent frequency of ice crystal habits is plotted as a function of distance from the top of the cirrus clouds (D_{top}) in Fig. 6.3. The panels in Fig. 6.3 are arranged according to the cloud top temperature (T_{top}). According to the cirrus observational dataset by Lawson et al. (2006a), the combination of D_{top} and T_{top} is not always a good indicator of particle shape and size, suggesting that new ice particles can nucleate and grow or sublimate at all levels in clouds. This behavior is generally similar to that of our cirrus dataset. However, there were some trends in the percent frequencies of ice crystal habits for T_{top}s colder than –55°C in spite of few cases of T_{top}s warmer than –55°C: the frequency of the plates tended to increase with increasing D_{top}, whereas that of bullets tended to decrease. Regardless of the T_{top}, bullet rosettes were most prevalent near cloud tops, the prevalence of side planes increased in the middle of the clouds, and the prevalence of plates had a tendency to increase with increasing D_{top}. In contrast, the frequency of the columns was greatest near cloud tops, and in some cases (Figs. 6.3b, 6.3e) the frequency of the columns tended to increase with increasing D_{top}.

6.2 Shape parameters

The axis ratio of column, bullet, and bullet rosette crystals measured with the HYVIS is shown in Fig. 6.4 as a function of dimension and temperature. The axis ratios of the column and bullet crystals had a tendency to decrease with increasing crystal dimension. However, there was little apparent correlation between the axis ratios of bullet rosettes and crystal dimension, suggesting that the growth of bullet rosettes tends to be isotropic. We found no clear temperature dependence of the axis ratio of the three crystal shapes. Similar to the axis ratios of the bullet rosettes, the axis ratios of the other three crystal shapes (plates, side planes, and combinations of columns and plates) were not strongly dependent on crystal dimension (not shown).

The area ratio of various types of ice crystal habits has been investigated in several

field projects and has been found a useful parameter for characterizing particle shapes in previous studies (M96, HM03). As in Fig. 6.4, the area ratios of the six crystal habits are plotted in Fig. 6.5, where they are compared with the analogous area ratios reported in previous studies. The size dependency of the area ratio decreases with increasing dimension for all crystal types at a decreasing rate with increasing dimension. The implications are that ice crystals have a more open geometry as they grow and that the area ratio gradually approaches a limit for the largest particle measured in the cloud. The general trend of the relationship between area ratio and crystal dimension for columnar crystals (Figs. 6.5a, 6.5b) in this study showed higher or similar trend compared with that in the HM03 study. The M96 curves in Figs. 6.5a and 6.5b predict a higher area ratio throughout the range of crystal dimensions than that apparent in the data, possibly due to differences in sampling conditions (e.g., the M96 data were generally sampled at warmer temperatures). The size dependencies of the area ratios of plates and side planes apparent in Figs. 6.5c and 6.5d were weak compared with the size dependencies of the other area ratios. A similar pattern is apparent in the results of other studies (M96, Me96, HK87, and HM03). In contrast, the decrease of the area ratio of bullet rosette crystals (Fig. 6.5e) with increasing crystal dimension was a stronger trend in this study than in previous one. Further investigation will be needed to identify the cause of this difference.

A significant trend was found in the relationship between the area ratio measured with the HYVIS and maximum dimension (Fig. 6.6a), its temperature (Fig. 6.6b), and normalized height (Fig. 6.6c), although the data points in Fig. 6.6 are widely scattered. A second-order polynomial fit to the mean area ratios in each 30 μm interval is shown in Fig. 6.6a. The value of the polynomial decreased from about 0.6 to 0.3 for 50 μm and 400 μm particles, respectively. These area ratios are smaller than the cirrus particle replicator data reported by HM03, but they evidence a trend that is generally similar to their results. Figure 6.6b shows a plot of area ratios for each temperature range in 10°C

intervals. The slope of the trend curve of area ratio versus maximum dimension was smaller in magnitude at warmer versus colder temperatures. Figure 6.6c shows plots of area ratios categorized according to cloud layer, each cloud is divided into five layers of equal thickness, from the cloud top to the cloud base. The slopes of the trend lines were steeper in the upper cloud layers than in the lower half of the clouds although the area ratios were highly variable. The height dependence in Fig. 6.6c is consistent with the temperature trends in Fig. 6.6b, which shows similar dependence to that in the HM03 study.

We applied the power–law relationships between particle dimensions and cross-sectional areas reported by M96 to the HYVIS data. Figure 6.7 shows the ratio of areas calculated from the empirical power–law equations (A_c) to areas measured from the image analysis (A_m) in each cirrus cloud layer (250 m height interval) whose temperature is assigned at mid-level in the layer. We found that the integral of A_c over the vertical column of a cloud could overestimate the integral of A_m by 10%–80%; the extent of overestimation was highly variable, irrespective of T_{top} or cloud depth (not shown). Although several different crystal habits contributed to the overestimation, this discrepancy was mainly due to the power laws (from M96) for columnar and bullet rosette types, as shown in Fig. 6.5.

6.3 Comparison with other datasets

During the past several decades, a variety of ice crystal habit diagrams have been drawn from laboratory studies, in situ observations (mainly on the ground), or combinations of the two. One of the most famous diagrams is the snow crystal morphology diagram (Nakaya 1954), which depicts a columnar habit at temperatures below –22°C. However, recent laboratory and field studies (BH09; Baker and Lawson 2006; Lawson et al. 2006a, 2006b) have both firmly established that the ice crystal habit

at temperatures between –40° to –20°C is plate-like and dominated by polycrystalline forms. This habit regime is consistent with our dataset, which evidenced significant frequencies of plates and side planes within this temperature range. The single bullet was also the dominant crystal habit in this temperature range in our dataset and was deemed to result from sedimentation of ice particles from colder regions aloft.

A significant difference in the present study and previous studies (Heymsfield et al. 2002; Lawson et al. 2006a, 2006b), is the abundance of single bullets. Single bullets originate from rosettes that break up. Gow (1965) reports that single bullets result from disintegration of bullet rosettes from sublimation. The disintegration is attributed to a gross weakening of the structure caused by sublimation at the center of the bullet clusters. One possibility of the high frequency of single bullets in our dataset is the difference of ice supersaturation compared with previous studies of in situ observations. The heads or apices of single bullets in the HYVIS images generally have a rounded shape. According to our simultaneous observations using the Snow White (chilled-mirror dewpoint sensor) during the 2004 and 2007 field campaigns, we had mostly near ice saturation to low ice supersaturation (–5% to <10%) in cloud layers, sometimes moderate to high ice supersaturation (10% to 30%), and sometimes ice subsaturation in the humidity profile. On the other hand, most studies by aircraft observations were typically made in vigorous clouds (with rather strong updraft) such as anvils, wave clouds, or precipitating frontal clouds. For a simplified comparison, all single bullet crystals in this study would be assumed to occur as a result of sublimation of bullet rosettes whose arms were 3 to 6 per bullet rosette on average; the averaged occurrence frequency of bullet rosettes would increase from 12% in the original dataset to 39%−32% in the assumed dataset, which is comparable with the observational result of Lawson et al (2006a). Another possibility is high frequency of breakup of bullet rosettes during sampling with the HYVIS, but this reasoning should be excluded by image analysis on a frame-by-frame

basis. The fragmented ice particles breaking up upon impact were excluded from the frequency of the ice crystal habit.

The ice particle images in our dataset consist of the great majority (>80%) of unclassified crystal habit type in particles smaller than 50 μm, as stated in section 6.1. We did not have the irregular type in our classification. The definition of irregular type remains unclear and varies in different studies, which makes it difficult to compare with previous studies in terms of the abundance of small irregular particles. Ice particles classified as the "rosette-shaped" type in the study by Lawson et al. (2006a) were classified mostly as bullet rosette or combination of columns and plates in this study. According to the findings of Baker and Lawson (2006) from the wave cloud observations, side planes were mostly observed on crystals that had exceeded their riming threshold size, suggesting that the side-plane growth may occur at a riming site via subsequent vapor deposition. In our cirrus dataset, there was no riming sign on ice particles, which is consistent with the laboratory study by BH04 that side planes can be observed even below water saturation conditions.

According to the study by BH04, ice crystal growth is influenced by factors such as defects, stress, and dislocations in a crystal, in addition to the main factors of temperature and ice supersaturation. The variability of growth rates causes the variability of the aspect (axis) ratios of columns or bullets commonly observed in cirrus clouds.

Figure 6.4 compares the axis ratios of columns and bullets in cirrus clouds measured with the HYVIS to the analogous ratios reported in previous studies (Heymfield 1972 (H72 in Fig. 6.4b) and MA94). In this study, we found wide variability of crystal axis ratios. On average the size dependency of the axis ratio of columnar crystals was similar to the size dependency reported in previous studies. Further analysis of aspect-ratio data in our dataset has yet to be performed for other types of ice crystals. For instance, the

aspect ratio of each element of a bullet rosette crystal can be compared with those reported in other studies and with those of single bullets or other elements in this study. BH04 states that component crystals of bullet rosettes often have non-uniform aspect ratios in the laboratory and that aspect ratios reported from in situ observations may be affected by vapor competition among neighboring component bullets and/or orientation during the fall of the crystal.

Figure 6.5 provides a comparison of the area ratios of several crystal types from HYVIS observations and previous studies. Another size dependency of the area ratio was apparent in the HYVIS dataset although there was wide variability for each crystal type. The M96 dataset was obtained from clouds with higher cloud top temperatures, the result perhaps being area ratios of columnar crystals larger than those in this study. Other reasons could be differences among microphysical instruments. The curves of single bullet crystals in the HM03 study were similar to the curves in this study, although the curves of the side planes differed between the two studies. These comparisons should be analyzed cautiously, because the area ratio is not simply determined by local temperatures and supersaturations in clouds but may also be influenced by other environmental factors (such as vertical velocity or relative humidity profiles) and by cloud macrophysical properties (such as cloud top temperature and/or cloud thickness).

The aspect (or axis) ratio or area ratio from 2D imaging probe data is subject to errors resulting from the rather coarse digitization (e.g., 25 μm resolution for the 2DC probe) of the particle images as well as to errors that depend on the orientation of the falling particle when it is imaged. The balloonborne videosonde (or ice crystal replicator) data have the advantage of being more finely resolved in addition to the CPI, although the latter errors are similarly included.

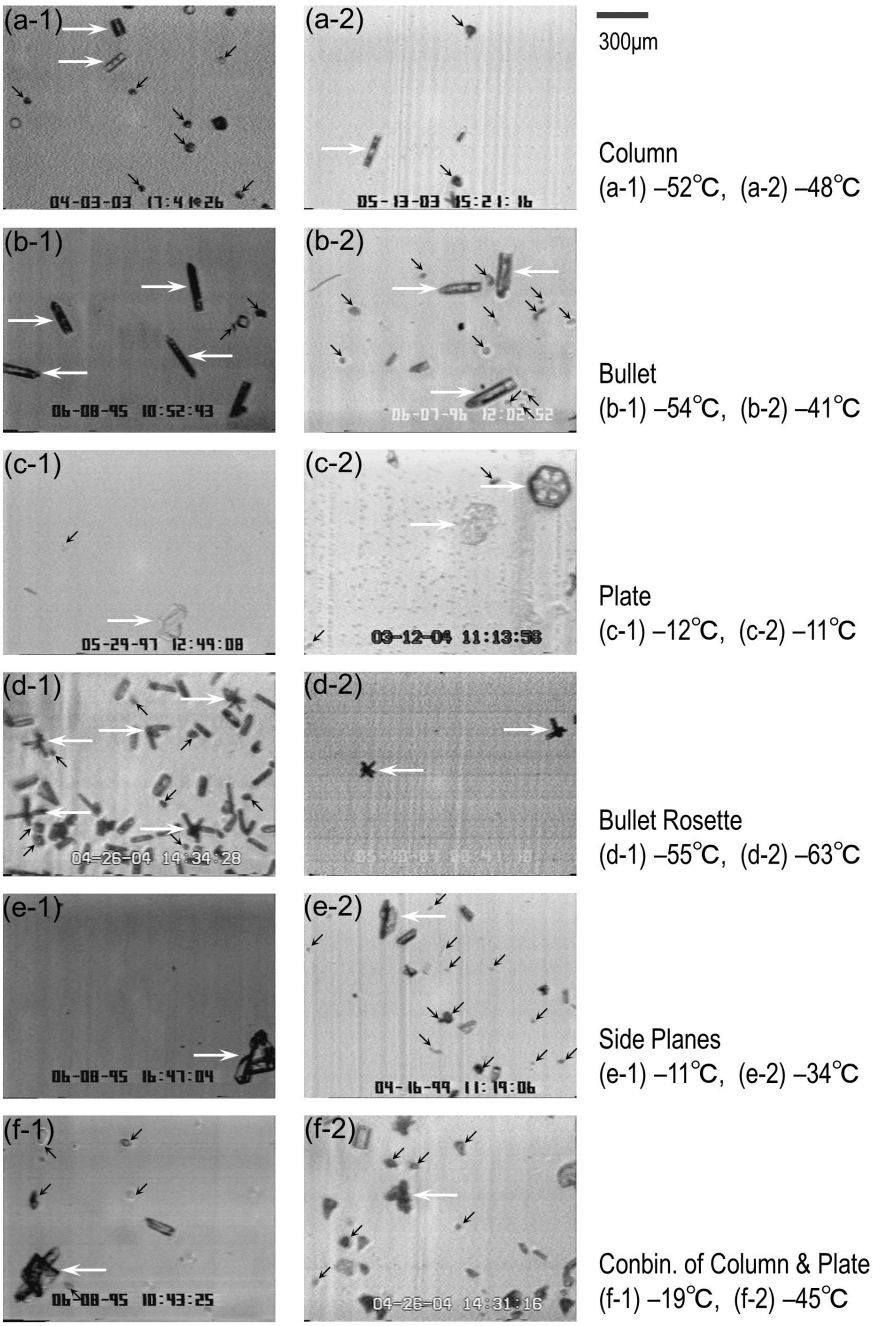

Fig 6.1 Examples of the HYVIS microscopic images observed in cirrus clouds in each classified type (two pictures in a row) of ice crystals (white arrows), accompanied with unclassified ice particles (black arrows). The ambient temperatures of each of two pictures in a classified type are indicated on the right-hand side.

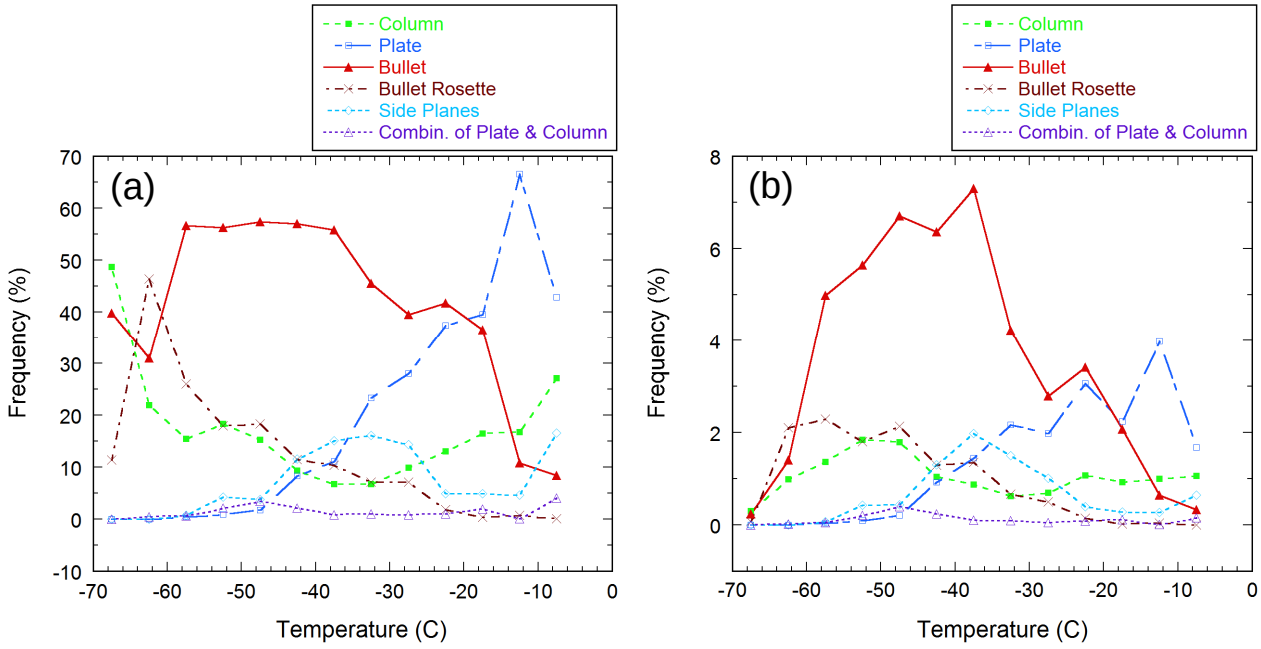

Fig 6.2 Percent frequency of occurrence of ice crystal habits as a function of ambient temperature. The frequencies have been normalized (a) within 5°C temperature intervals or (b) by total counts regardless of temperature.

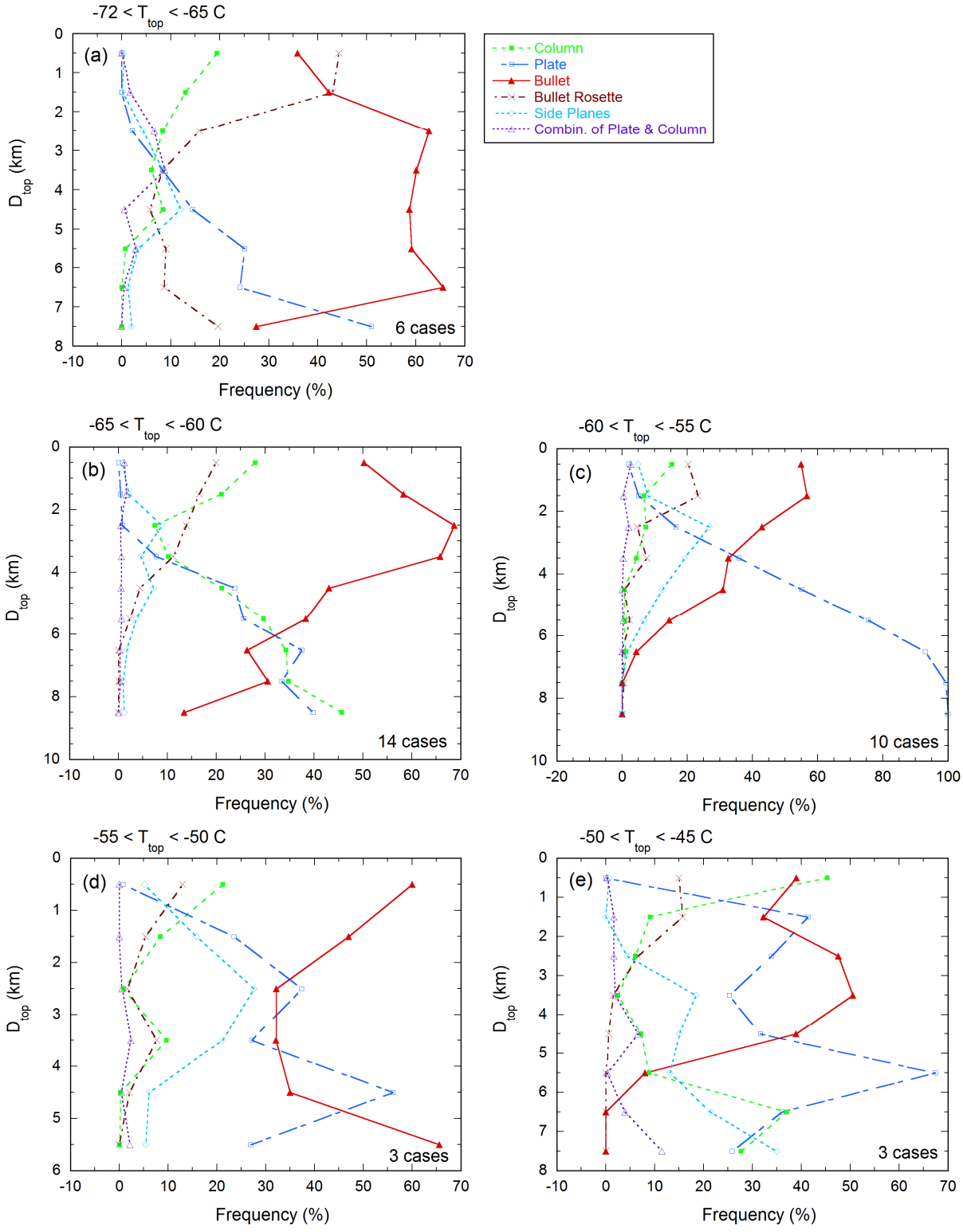

Fig 6.3 Same as Fig. 6.2, but as a function of distance from cirrus cloud tops. The frequencies have been normalized within a 1 km cloud depth interval. The plots have been sorted on the basis of the cloud top temperature.

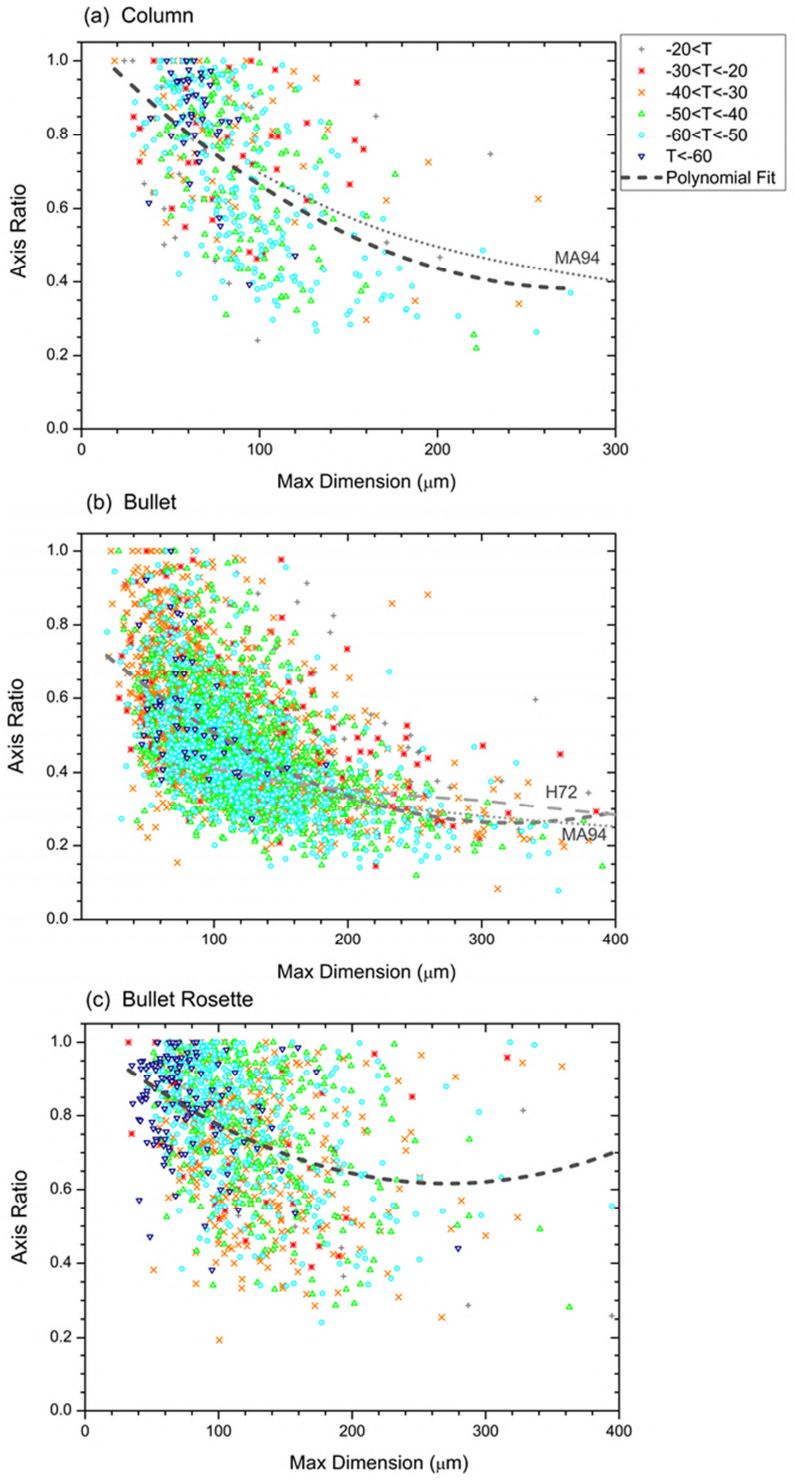

Fig 6.4 Relationships between axis ratios and maximum dimensions for crystal habits in the shape of (a) columns, (b) bullets, and (c) bullet rosettes. Data points have been shaded according to the ambient temperature. Only data for microscopic images were analyzed. The dark, short-dashed curve in each panel is a second-order polynomial fit to the HYVIS data. The analogous curves from H72 (long dashes) and MA94 (dots) are shown for comparison.

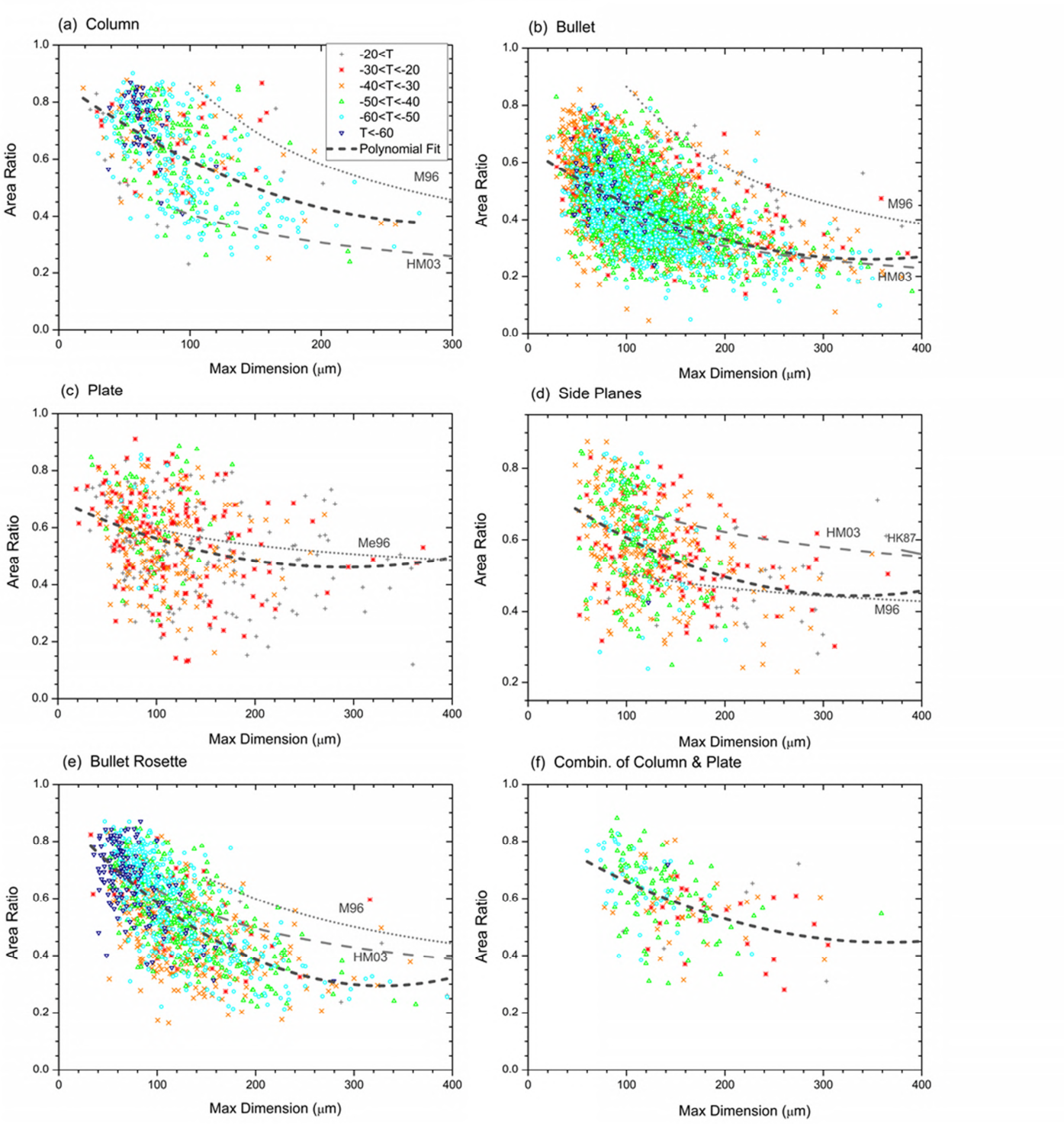

Fig 6.5 Same as Fig. 6.4, but for area ratios of crystal habits in the form of (a) columns, (b) bullets, (c) plates, (d) side planes, (e) bullet rosettes, and (f) combinations of columns and plates. The analogous curves from M96 (dots), Me96 (dots), HK87 (solid curve), and HM03 (long dashes) are shown for comparison.

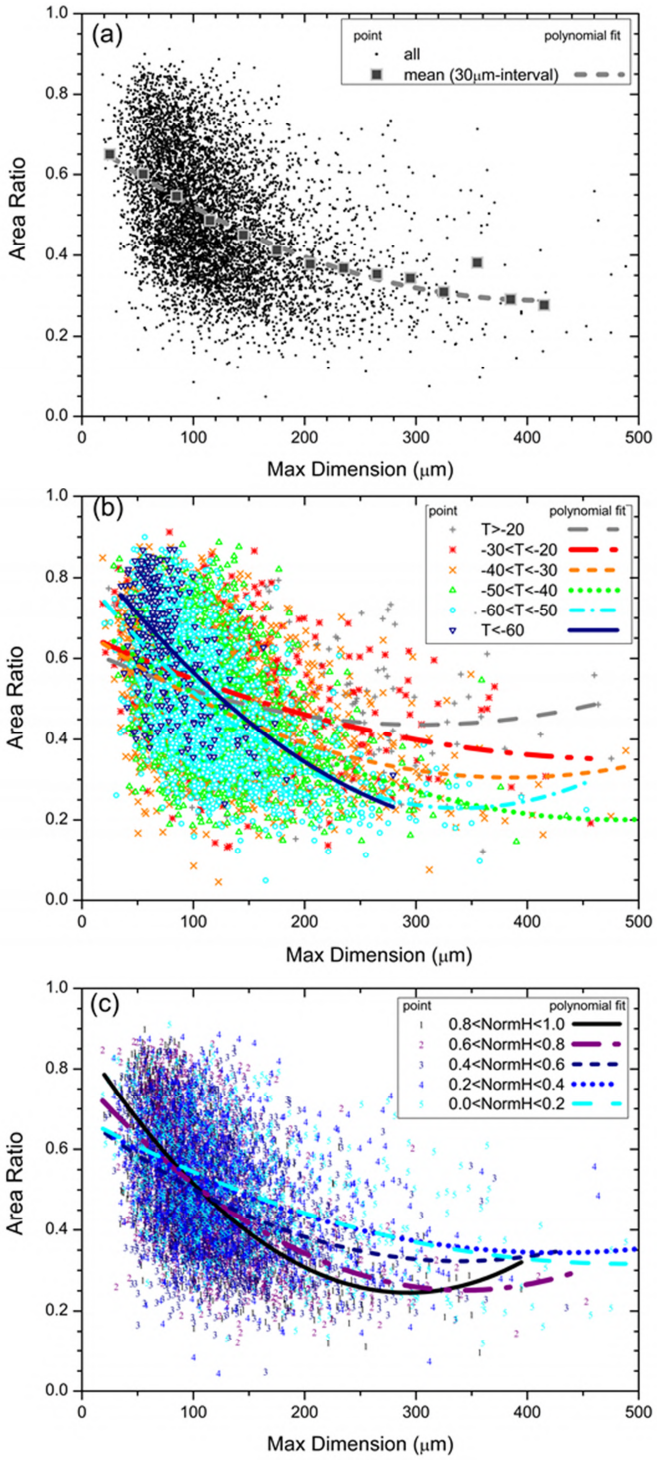

Fig 6.6 Relationship between area ratios and maximum dimensions. The curves are second-order polynomials fit to the HYVIS data points grouped on the basis of (a) the mean values (squares) within 30 μm intervals (excluding an outlier point, which corresponds to the 340–370 μm interval); (b) the indicated temperature intervals; or (c) five cloud layers, each cloud is divided into layers of equal thickness between the cloud base and the cloud top.

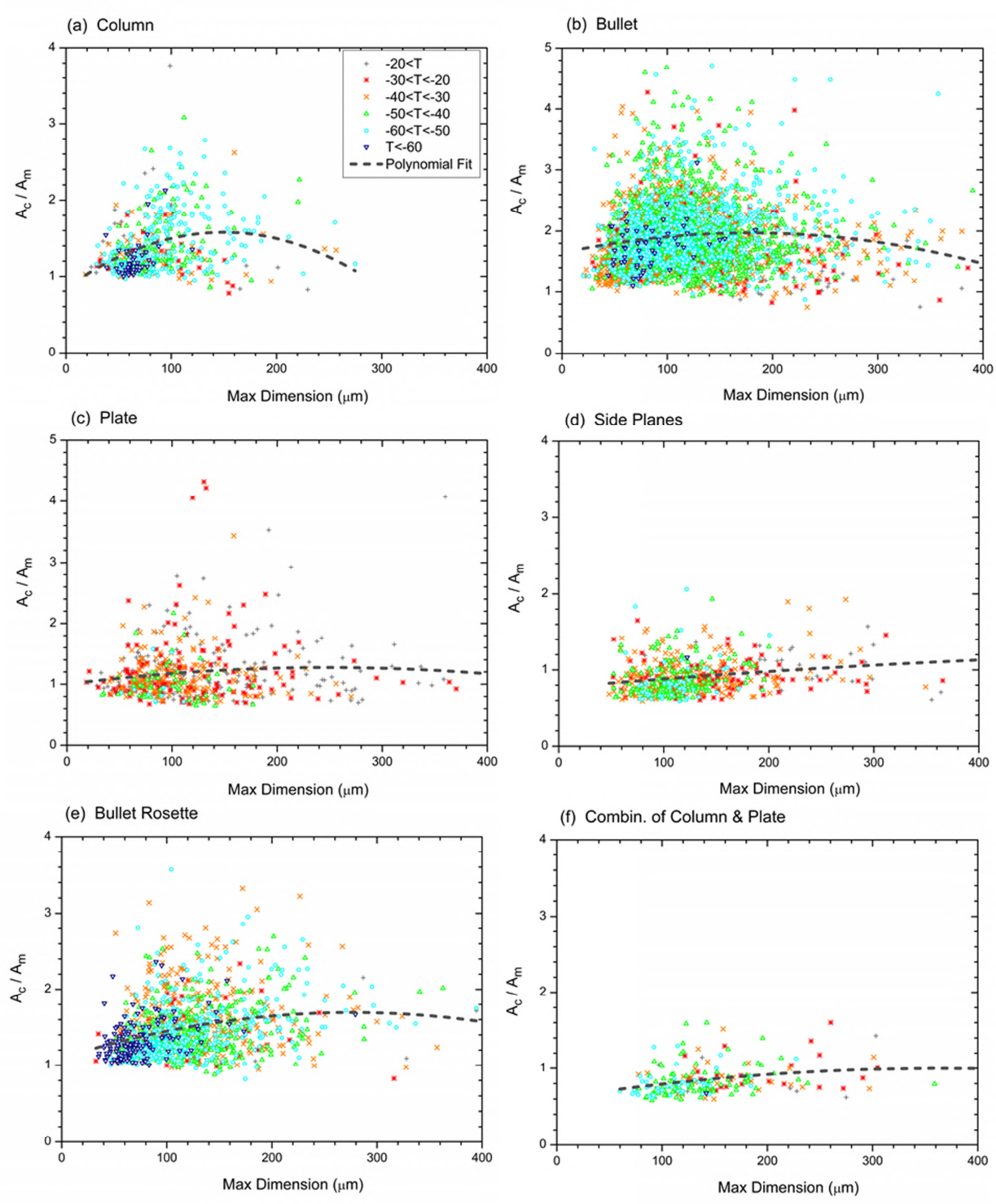

Fig 6.7 Ratio of cross-sectional areas (A_c) calculated from the empirical power laws reported by Mitchell (1996) to the measured cross-sectional areas (A_m) determined from analyses of the images in each cirrus cloud layer (250 m height intervals).

7. Summary and conclusions

A new version of Hydrometeor Videosonde (HYVIS) for measuring cirrus clouds was developed. By adding a suction fan, sufficient sampling volume could be obtained to determine the form of size distributions at 250-m height intervals in cirrus clouds with low ice crystal concentrations. Adding a suction fan greatly enhances the collection efficiencies for smaller particles and enables reliable ice crystal spectra for sizes down to 10 μm to be obtained. The new HYVIS measurements also provide information on detailed shapes of ice crystals. They should lead to advanced studies on microphysical structures and radiative properties in cirrus clouds and increase our understanding of mechanisms for the formation and maintenance of cirrus clouds.

Firstly, we reported on ice crystal concentrations measured in synoptically-generated cirrus clouds by a balloonborne videosonde, which has the advantage of more reliably measuring small ice crystals in the size range of 10–100 μm than the conventional aircraft instruments. We have collected a unique dataset of cirrus ice particle concentrations from nearly 40 launches of the HYVIS. The comparison tests between the HYVIS and other airborne microphysical instruments, conducted in the laboratory, suggested that the CE of the HYVIS had an uncertainty factor of 2–3 for 10–30 μm particles and less than 2 for particles larger than 30 μm. From the degree of uncertainty in the *CE* of the HYVIS, the observed broad size distributions of ice crystals, and low ice-supersaturation conditions, we conclude that the measurements presented in this study do not substantially underestimate the total concentration, although there exists some uncertainty about the concentration measurements at particle sizes smaller than 30 μm.

One of the focuses in this study was to report on the concentrations of ice crystals in cirrus as they relate to cloud radiation. The vertical distributions of the ice crystal concentrations were found to be roughly constant, except for those near the cloud top and

base. Although the maximum concentrations were located mostly (~35%) near the cloud top ($NormH \geq 0.8$) among five equally partitioned cloud layers, they occurred at various vertical locations; there was no correlation between the cloud depth and the normalized height or the distance from the cloud top, where the maximum concentrations occurred. Typical concentrations were of the order of 10 to 100 L^{-1}. The relative humidity profiles in the vertical combined with the associated frequency of occurrence of the various crystal habits, suggest that sublimation should be responsible for the observed increase in the frequency of single bullets near the cloud base and there was an enhancement in the concentrations near the cloud base in some cases.

A comparison between ice crystal concentrations measured with the HYVIS and simulated with parcel cloud models has helped in the interpretation of the ice nucleation mechanisms in these cirrus clouds. From this comparison, homogeneous ice nucleation produces concentrations of the order of 1 to 10 cm^{-3}, which is significantly higher than our measured result and strongly dependent on temperature. It was noteworthy that the concentration measurements did not indicate such strong dependence on temperature, even near the cloud top where many ice crystals were supposed to be nucleated. The results suggest that various physical processes are involved in the vertical profile of ice crystal concentrations; the concentration decreases owing to ice crystal growth and its fallout; on the other hand, it increases owing to heterogeneous ice nucleation and/or ice particle breakup.

In the parcel model simulations presented here and perhaps in clouds, the homogeneous ice nucleation process ceases shortly after the peak RH is attained. The size distribution should then shift to larger sizes in response to ice crystal growth and fallout producing a narrow size distribution, in which the concentration falls off rapidly at small sizes. Thereafter, additional crystals may be produced by heterogeneous nucleation or a type of breakup mechanism, leading to a broad size distribution. Because we often

observed broad size distributions (at least down to 10 μm), the heterogeneous nucleation process or a breakup mechanism is necessary to explain the observations.

However, there are several uncertainties that make it difficult to conclude whether homogeneous or heterogeneous ice nucleation was the dominant mechanism operated in the clouds under study. First, the concentrations of ice crystals nucleated by homogeneous nucleation are critically dependent on the updraft velocity, and we are not aware of the values of vertical velocity in the observed clouds. Second, substantial uncertainties are included in numerical simulations of cirrus formation through the homogeneous nucleation process, as suggested by early studies. Moreover, there were no measured data in the clouds under study suggesting any information of primary importance about the cirrus initiation processes, such as physical and chemical properties of aerosols (serving as CCN and IN), peak relative humidity, and updraft velocity. These data will be highly useful for further understanding the cirrus formation mechanisms. With these desired datasets, recent modeling and laboratory studies would also greatly help to interpret in situ microphysical measurements of cirrus clouds.

Secondly, the contribution of small ice crystals (<100 μm) to the IWC (mass) or A_c (area or extinction) in observed cirrus clouds was examined. The dataset in this study is considered to be less affected of artifacts compared with the conventional FSSP-type instrument. The averaged contribution in size of D < 50 μm tended to decrease as the total A_c or IWC became larger, while that in size ranges of D > 100 μm tended to increase. The contribution to the total in size range of 100 < D < 200 μm became most dominant for A_c larger than 0.05 mm^2/L and for IWC larger than 0.0005 g/m^3. In the HYVIS dataset, the averaged contributions of ice crystals with 10 < D < 50 μm to the total NC, A_c, and IWC were 53%, 19%, and 13%, respectively. These statistics suggested that the small ice crystals had little impact on the mass or extinction in cirrus clouds in this study, compared with results of the previous studies – even after excluding the possible

small-particle artifacts due to shattering of large ice crystals.

Thirdly, we reported on the frequency of the occurrence of ice crystal habits in midlatitude cirrus clouds measured with the HYVIS. The bullet type crystal was predominant at temperatures between –60° and –20°C. The possibility of high frequency of single bullets in this study is related to the sampling humidity conditions — near ice saturation to low ice supersaturation. At temperatures colder than –40°C, the average frequency of bullet rosette and column types increased with decreasing temperature, whereas at temperatures warmer than –40°C, the frequency of the plate types increased with increasing temperature. These results are consistent with recent laboratory studies. Plots of habit frequency versus cloud depth, sorted by cloud top temperature, revealed that the habit frequency distribution was influenced mainly by ambient temperature, with some effects caused by sedimentation. It should be noted, however, that there is no information in the HYVIS dataset that could be used to isolate effects of other factors, such as ice supersaturation, updraft velocity, and ice nucleation onto aerosols.

Shape-sensitive parameters, such as the area ratio or aspect (axis) ratio, can facilitate deduction of more accurate information about the microphysical and optical properties of ice clouds. We examined the size and temperature dependencies of area ratios and axis ratios determined from the HYVIS measurements and compared those dependencies with results from previous studies. Similarities were generally found in the size and temperature dependencies; however, further studies are required to analyze the differences between our results and those from previous studies and to explain the large variability within the same dataset. A large error in the total cross-sectional area of the population of ice particles (and in the extinction coefficient of clouds) might be introduced using the conventional power–law relationships between area and dimension. These uncertainties can be attributed to the differences in relationships from one dataset to another and to the substantial natural variability in the relationships. Normalized cloud

height, as well as the temperature and crystal shape, can influence the relationship between the area ratio and size.

The characteristics of ice crystal habits and shape-sensitive parameters obtained in this study are basic information about natural cirrus clouds and can be used to assess differences between datasets and/or between individual cases. However, the characteristics are not well known. Laboratory and theoretical studies of ice particle growth and evaporation are required to better understand the distribution of crystal shapes and the substantial variability in the vertical distributions and size dependency of shape-sensitive parameters derived from the HYVIS dataset.

The HYVIS dataset in this study has an advantage of reliable in situ measurements of cirrus ice crystals smaller than 100 μm, which makes the dataset unique to other field campaign datasets available. In this study the microphysical properties measured with the HYVIS, generally associated with synoptical depressions, were uniquely characterized in terms of number concentrations or size distributions of ice crystals, contributions of small ice crystals to cirrus mass or extinction, and ice crystal shapes. The HYVIS instrument is one of the most powerful and unique technique for microphysical measurements in cirrus clouds. The measured microphysical properties are fundamental to reliably quantify radiative properties of cirrus clouds.

ACKNOWLEDGMENTS

The author wishes to express his sincere gratitude to Prof. Hiroshi Uyeda, Nagoya University, for his guidance and constructive suggestions throughout the preparation of this thesis.

The author would like to express his heartfelt gratitude to Dr. Masataka Murakami, Meteorological Research Institute (MRI), for his continuous support, encouragement, and sincere guidance throughout this study and in my research career. My deep gratitude also goes to Mr. Toyoaki Tanaka, who introduced me to the field of cloud physics and supported me through my earliest attempts to become a member of the profession.

The author wishes to thank the staff of the Tateno Aerological Observatory, Japan Meteorological Agency, and Mr. Hakaru Mizuno, Dr. Yoshinori Yamada, Dr. Kenichi Kusunoki, Ms. Mizuho Hoshimoto, and the Cloud Physics Laboratory staff of the MRI for their cooperation in the balloonborne observations. My special thanks must also go to assistant staff of the Cloud Physics Laboratory for analyzing the HYVIS image data. The author would like to express his thanks to the staff of Meisei Electric Co. for their great support during the development of the HYVIS. The author is also grateful the technical staff at the Wind Tunnel Facility of the MRI for their cooperation in sampling volume experiments.

I extend my sincere gratitude to Drs. Shoji Asano, Akihiro Uchiyama, and Teruo Aoki for their valuable comments, and to Drs. Akihiro Yamazaki, Tomohiro Nagai, Tetsu Sakai, Ahoro Adachi for providing me with their remote-sensing data.

This study was partly conducted during my visit to National Center for Atmospheric Research (NCAR) in USA. I would like to express my sincere gratitude to Dr. Andrew. J. Heymsfield for his invaluable suggestions and advice. I am grateful to Drs. David. C. Rogers, Paul. J. DeMott, Greg. M. McFarquhar, Paul. R. Field for their fruitful

discussions. Thanks are due to Drs. L. M. Miloshevich and A. Bansemer for providing me with their replicator data and program.

This study was primarily done as a part of the Japanese Cloud and Climate Study (JACCS) program which was supported by the Science and Technology Agency of Japanese Government.

Appendix : Comparison between HYVIS and other instruments

The HYVIS captures images of the hydrometeors whose sizes are larger than 10-μm diameter. For water droplets, there was a relatively sharp increase in the collection efficiency (*CE*) of the HYVIS at diameters between 10 and 20 μm compared to the FSSP measurements in an artificial fog of droplets smaller than 100 μm in our laboratory. The *CE* was considered to reach unity before the droplet size increased to 20 μm. For sampling of ice particles, the actual *CE* should be confirmed and evaluated, which is dominantly influenced by stickiness of a collecting surface coated with silicone oil.

Unfortunately, neither standardized instruments nor techniques are recognized for measuring concentrations of small ice particles (<100 μm). The HYVIS measurements were compared with the SPEC CPI (version 2) measurements as a reference for ice crystals formed in our laboratory. Ice fog was artificially prepared in a cold room by glaciating supercooled fog with a small piece of dry ice. The size of ice particles ranged from several microns to 100–200 μm. To minimize the uncertainty of the sample area of the CPI, a cylindrical sample nozzle with an inner diameter of 2 mm was attached to the inlet in such a way that the nozzle axis was aligned with respect to the optical center of the CPI's particle detection system.

The ratio of particle number concentrations measured with the HYVIS and CPI increased with size in the range of 10–30 μm; the average value of the ratio increased from about 0.5 to 1.5 (with deviation from 0.3 to 3) over the size range. We also found that the actual *CE* of the HYVIS for ice crystals larger than 30 μm agreed with the theoretical estimate within an uncertainty factor of 2. However, further experiments (with a more reliable instrument and technique) are needed for quantitative estimation of the *CE* in the size range of 10–30 μm.

The HYVIS would greatly underestimate ice crystal concentrations when it is used for measuring cirrus clouds where ice germs smaller than 10 μm are dominantly present, for

example, some anvils or cirrus clouds at an early stage of their life cycle. As shown in Fig. 4.2, the size distributions in the HYVIS dataset were not extremely steep at sizes smaller than 30 μm. This feature would be responsible for little difference between total concentrations including and excluding particles in the size range of 10–30 μm in Fig. 4.3. Thus, we believe that the uncertainty of the *CE* should have a rather small impact on the total concentrations of ice crystals larger than 10 μm for the dataset presented in this study because the *CE* of the HYVIS over this size range does not change by more than a factor of 2.

REFERENCES

Asano, S., JACCS/MRI Research Group, 1994: Japanese Cloud Climate Study (JACCS): Research plan and preliminary results. *Preprint of the 8th Conf. Atmos. Radiation, Nashville, TN, U.S.A., Amer. Meteor. Soc.*, 282–284.

Asano, S., and JACCS Cirrus Observation Team, 1997: A sonde system for simultaneous measurements of radiative and cirrus microphysics in the Japanese Cloud-Climate Study (JACCS) program. *IRS'96: Current Problems in Atmospheric Radiation* (W. L. Smyth and K. Stamnes, Eds.), A. Deepak Publishing, Hampton, VA, 349–352.

Bailey, M., and J. Hallett, 2004: Growth rates and habits of ice crystals between –20° and –70°C. *J. Atmos. Sci.*, **61**, 514–554.

Bailey, M., and J. Hallett, 2009: A comprehensive habit diagram for atmospheric ice crystals: Confirmation from the laboratory, AIRS II, and other field studies. *J. Atmos. Sci.*, **66**, 2888–2899.

Baker, B. A., and R. P. Lawson, 2006: In situ observations of the microphysical properties of wave, cirrus, and anvil clouds. Part I: Wave clouds. *J. Atmos. Sci.*, **63**, 3160–3185.

Barton, I. J., 1983: Upper level cloud climatology from orbiting satellite. *J. Atmos. Sci.*, **40**, 435-447.

Baumgardner, D., and Coauthors, 2012: In situ, airborne instrumentation: Addressing and solving measurement problems in ice clouds. *Bull. Amer. Meteor. Soc.*, **93**, ES29–ES34.

Connolly, P. J., M. J. Flynn, Z. Ulanowski, T. W. Choularton, M. W. Gallagher, and K. N. Bower, 2007: Calibration of the cloud particle imager probes using calibration beads and ice crystal analogs: the depth of field. *J. Atmos. Oceanic Technol.*, **24**, 1860–1879.

Davis, C. I., 1974: The ice-nucleating characteristics of various AgI aerosols. *Ph. D. thesis*, University of Wyoming, 267 pp.

DeMott, P. J., 2002: Laboratory studies of cirrus cloud processes. *Cirrus* (D. K. Lynch, K. Sassen, D. O'C. Starr, and G. Stephens, Eds.), Oxford University Press, New York, 102–135.

DeMott, P. J., 2007: Progress and issues in quantifying ice nucleation involving atmospheric aerosols. *Nucleation and Atmospheric Aerosols* (C. D. O'Dowd and P. E. Wagner, Eds.), Springer, 405–417.

DeMott, P. J., M. P. Meyers, and W. R. Cotton, 1994: Parameterization and impact of ice initiation processes relevant to numerical model simulations of cirrus clouds. *J. Atmos.*

Sci., **51**, 77–90.

DeMott, P. J., D. C. Rogers, and S. M. Kreidenweis, 1997: The susceptibility of ice formation in upper tropospheric clouds to insoluble aerosol components. *J. Geophys. Res.*, **102**, 19575–19584.

DeMott, P. J., and Coauthors, 2010: Predicting global atmospheric ice nuclei distributions and their impacts on climate. *Proc. Natl. Acad. Sci.*, USA, **107**, 11217–11222, doi:10.1073/pnas.0910818107.

Dong, Y., R. G. Oraltay, and J. Hallett, 1994: Ice particle generation during evaporation. *Atmos. Res.*, **32**, 45–53.

Dowling, D. R., and L. F. Radke, 1990: A summary of the physical properties of cirrus clouds. *J. Appl. Meteor.*, **29**, 970–978.

Eidhammer, T., P. J. DeMott, and S. M. Kreidenweis, 2009: A comparison of heterogeneous ice nucleation parameterizations using a parcel model framework. *J. Geophys. Res.*, **114**, D06202, doi:10.1029/2008JD011095.

Field, P. R., R. Wood, P. R. A. Brown, P. H. Kaye, E. Hirst, R. Greenaway, and J. A. Smith, 2003: Ice particle interarrival times measured with a Fast FSSP. *J. Atmos. Oceanic Technol.*, **20**, 249–261.

Field, P. R., A. J. Heymsfield, and A. Bansemer, 2006: Shattering and particle interarrival times measured by optical array probes in ice clouds. *J. Atmos. Oceanic Technol.*, **23**, 1357–1370.

Fletcher, N. H., 1962: *Physics of Rain Clouds.* Cambridge University Press, 386pp.

Francis, P. N., J. S. Foot, and A. J. Baran (1999), Aircraft measurements of the solar and infrared radiative properties of cirrus and their dependence on ice crystal shape, *J. Geophys. Res.*, **104**, 31685–31695.

Fukuta, N., and L. A. Walter, 1970: Kinetics of hydrometeor growth from a vapor-spherical model. *J. Atmos. Sci.*, **27**, 1160–1172.

Gardiner, B. A., and J. Hallett, 1985: Degradiation of in-cloud forward scattering spectrometer probe measurements in the presence of ice particles. *J. Atmos. Oceanic Technol.*, **2**, 171–180.

Garrett, T. J., H. Gerber, D. G. Baumgardner, C. H. Twohy, and E. M. Weinstock, 2003: Small, highly reflective ice crystals in low-latitude cirrus, *Geophys. Res. Lett.*, **30**, 2132, doi:10.1029/2003GL018153.

Gayet, J.-F., G. Febvre, and H. Larsen, 1996: The reliability of the PMS FSSP in the presence of small ice crystals. *J. Atmos. Oceanic Technol.*, **13**, 1300–1310.

Gierens, K., 2003: On the transition between heterogeneous and homogeneous freezing. *Atmos. Chem. Phys.*, **3**, 437-446.

Gierens, K., M. Monier, and J.-F. Gayet, 2003: The deposition coefficient and its role for cirrus clouds. *J. Geophys. Res.*, **108**, 4069, doi:10.1029/2001JD001558.

Gow, A. J., 1965: On the origin of bullet crystals at the South Pole. *J. Glaciol.*, **16**, 461–465.

Hallett, J., 1976: Measurements of size, concentration and structure of atmospheric particulates by the airborne continuous particle replicator. *Air Force Geophysics Laboratory Tech. Rep.*, AFGL–TR–76–0149, 151pp.

Heymsfield, A. J., 1972: Ice crystal terminal velocities. *J. Atmos. Sci.*, **29**, 1348–1357.

Heymsfield, A. J., and C. M. R. Platt, 1984: A parameterization of the particle size spectrum of ice clouds in terms of the ambient temperature and ice water content. *J. Atmos. Sci.*, **41**, 846–855.

Heymsfield, A. J., and M. Kajikawa, 1987: An improved approach to calculating terminal velocities of plate-like crystals and graupel. *J. Atmos. Sci.*, **44**, 1088–1099.

Heymsfield, A. J., and R. M. Sabin, 1989: Cirrus crystal nucleation by homogeneous freezing of solution droplets. *J. Atmos. Sci.*, **46**, 2252–2264.

Heymsfield, A. J., and L. M. Miloshevich, 1993: Homogeneous ice nucleation and supercooled liquid water in orographic wave clouds. *J. Atmos. Sci.*, **50**, 2335–2353.

Heymsfield, A. J., and L. M. Miloshevich, 1995: Relative humidity and temperature influences on cirrus formation and evolution: Observations from wave clouds and FIRE II. *J. Atmos. Sci.*, **52**, 4302–4326.

Heymsfield, A. J., and G. M. McFarquhar, 1996: High albedos of cirrus in the tropical Pacific warm pool: Microphysical interpretations from CEPEX and from Kwajalein, Marshall Islands. *J. Atmos. Sci.*, **53**, 2424–2451.

Heymsfield, A. J., and L. M. Miloshevich, 2003: Parameterizations for the cross-sectional area and extinction of cirrus and stratiform ice cloud particles. *J. Atmos. Sci.*, **60**, 936–956.

Heymsfield, A. J., S. Lewis, A. Bansemer, J. Iaquinta, L. M. Miloshevich, M. Kajikawa, C. Twohy, and M. R. Poellot, 2002: A general approach for deriving the properties of cirrus and stratiform ice cloud particles. *J. Atmos. Sci.*, **59**, 3–29.

Ivanova, D., D. L. Mitchell, W. P. Arnott, and M. Poellot, 2001: A GCM parameterization for bimodal size spectra and ice mass removal rates in mid-latitude cirrus clouds. *Atmos. Res.*, **59–60**, 89–113.

Jensen, E. J., and O. B. Toon, 1997: The potential impact of soot particles from aircraft exhaust on cirrus clouds. *Geophys. Res. Lett.*, **24**, 249–252.

Jensen, E. J., and Coauthors, 1998: Ice nucleation processes in upper tropospheric wave-clouds observed during SUCCESS. *Geophys. Res. Lett.*, **25**, 1363–1366.

Jensen, E. J., and Coauthors, 2009: On the importance of small ice crystals in tropical anvil cirrus. *Atmos. Chem. Phys.*, **9**, 5519–5537.

Korolev, A. V., E. F. Emery, J. W. Strapp, S. G. Cober, G. A. Isaac, M. Wasey, and D. Marcotte, 2011: Small ice particles in tropospheric clouds: fact or artifact? Airborne Icing Instrumentation Evaluation Experiment. *Bull. Amer. Meteor. Soc.*, **92**, 967–973.

Kristjánsson, J. E., J. M. Edwards, and D. L. Mitchell, 2000: Impact of a new scheme for optical properties of ice crystals on climates of two GCMs. *J. Geophys. Res.*, **105**, 10063–10080.

Lawson, R. P., 2011: Effects of ice particles shattering on the 2D-S probe. *Atmos. Meas. Tech.*, **4**, 1361–1381.

Lawson, R. P., A. J. Heymsfield, S. M. Aulenbach, and T. L. Jensen, 1998a: Shapes, sizes and light scattering properties of ice crystals in cirrus and a persistent contrail during SUCCESS. *Geophys. Res. Lett.*, **25**, 1331–1334.

Lawson, R. P., A. V. Korolev, S. G. Cober, T. Huang, J. W. Strapp, and G. A. Isaac, 1998b: Improved measurements of the drop size distribution of a freezing drizzle event. *Atmos. Res.*, **47–48**, 181–191.

Lawson, R. P., B. A. Baker, C. G. Schmitt, and T. L. Jensen, 2001: An overview of microphysical properties of Arctic clouds observed in May and July 1998 during FIRE ACE. *J. Geophy. Res.*, **106**, 14989–15014.

Lawson, R. P., B. A. Baker, B. Pilson, and Q. Mo, 2006a: In situ observations of the microphysical properties of wave, cirrus, and anvil clouds. Part II: Cirrus clouds. *J. Atmos. Sci.*, **63**, 3186–3203.

Lawson, R. P., B. A. Baker, P. Zmarzly, D. O'Connor, Q. Mo, J.-F. Gayet, and V. Shcherbakov, 2006b: Microphysical and optical properties of atmospheric ice crystals at South Pole Station. *J. Appl. Meteor. Climatol.*, **45**, 1505–1524.

Lawson, R. P., D. O'Connor, P. Zmarzly, K. Weaver, B. A. Baker, Q. Mo, and H. Jonsson, 2006c: The 2D-S (Stereo) probe: design and preliminary tests of a new airborne, high-speed, high-resolution particle imaging probe. *J. Atmos. Oceanic Technol.*, **23**, 1462–1477.

Lin, R.-F., D. O'C. Starr, P. J. DeMott, R. Cotton, K. Sassen, E. Jensen, B. Kärcher, and X.

Liu, 2002: Cirrus parcel model comparison project. Phase 1: The critical components to simulate cirrus initiation explicitly. *J. Atmos. Sci.*, **59**, 2305–2329.

Liou, K. N., 1986: Influence of cirrus clouds on weather and climate processes: A global perspective. *Mon. Wea. Rev.*, **114**, 1167–1199.

Magee, N., A. M. Moyle, and D. Lamb, 2006: Experimental determination of the deposition coefficient of small cirrus-like ice crystals near –50°C. *Geophys. Res. Lett.*, **33**, L17813, doi:10.1029/2006GL026665.

Magono, C., and C. W. Lee, 1966: Meteorological classification of natural snow crystals. *Journal of Faculty of Science, Hokkaido University, Ser. VII (Geophysics), Vol. 2*, 321–335.

Magono, C., and S. Tazawa, 1966: Design of "snow crystal sonde". *J. Atmos. Sci.*, **23**, 618-625.

McFarquhar, G.M., J. Um, M. Freer, D. Baumgardner, G.L. Kok and G. Mace, 2007: Importance of small ice crystals to cirrus properties: Observations from the Tropical Warm Pool International Cloud Experiment (TWP-ICE). *Geophys. Res. Lett.*, **34**, L13803, doi:10.1029/2007GL02986.

Meyers, M. P., P. J. DeMott, and W. R. Cotton, 1992: New primary ice nucleation parameterizations in an explicit cloud model. *J. Appl. Meteor.*, **31**, 708–721.

Miloshevich, L. M., and A. J. Heymsfield, 1997: A balloon-borne continuous cloud particle replicator for measuring vertical profiles of cloud microphysical properties: Instrument design, performance, and collection efficiency analysis. *J. Atmos. Oceanic Technol.*, **14**, 753–768.

Miloshevich, L. M., H. Vömel, A. Paukkunen, A. J. Heymsfield, and S. J. Oltmans, 2001: Characterization and correction of relative humidity measurements from Vaisala RS80–A radiosondes at cold temperatures. *J. Atmos. Oceanic Technol.*, **18**, 135–156.

Mishchenko, M. I., W. B. Rossow, A. Macke, and A. A. Lacis, 1996: Sensitivity of cirrus cloud albedo, bidirectional reflectance and optical thickness retrieval accuracy to ice particle shape. *J. Geophys. Res.*, **101**, 16973–16985.

Mitchell, D. L., 1996: Use of mass- and area-dimensional power laws for determining precipitation particle terminal velocities. *J. Atmos. Sci.*, **53**, 1710–1723.

Mitchell, D. L., and W. P. Arnott, 1994: A model predicting the evolution of ice particle size spectra and radiative properties of cirrus clouds. *J. Atmos. Sci.*, **51**, 817–832.

Mitchell, D. L., A. Macke, and Y. Liu, 1996: Modeling cirrus clouds. Part II: Treatment of radiative properties. *J. Atmos. Sci.*, **53**, 2967–2988.

Mizuno, H., T. Matsuo, M. Murakami and Y. Yamada, 1994: Microstructure of cirrus clouds observed by HYVIS. *Atmos. Res.*, **32**, 115–124.

Murakami, M., and T. Matsuo, 1990: Development of the hydrometeor videosonde. *J. Atmos. Oceanic Technol.*, **7**, 613–620.

Murakami, M., T. Matsuo, T. Nakayama and T. Tanaka, 1987: Development of cloud particle video sonde. *J. Meteor. Soc. Japan*, **65**, 803-809.

Nakaya, U, 1954: *Snow Crystals, Natural and Artificial.* Harvard University Press, Cambridge, 510 pp.

Orikasa, N., and M. Murakami, 1997: A new version of hydrometeor videosonde for cirrus cloud observations. *J. Meteor. Soc. Japan*, **75**, 1033–1039.

Ranz, W. E., and J. B. Wong, 1952: Impaction of dust and smoke particles on surface and body collectors. *Ind. Eng. Chem.*, **44**, 1371–1381.

Sassen, K., and G. C. Dodd, 1988: Homogeneous nucleation rate for highly supercooled cirrus cloud droplets. *J. Atmos. Sci.*, **45**, 1357–1369.

Sassen, K., and G. C. Dodd, 1989: Haze particle nucleation simulations in cirrus clouds, and applications for numerical modeling and lidar studies. *J. Atmos. Sci.*, **46**, 3005–3014.

Sassen, K., and J. R. Campbell, 2001: A midlatitude cirrus cloud climatology from the facility for atmospheric remote sensing. Part I: Macrophysical and synoptic properties. *J. Atmos. Sci.*, **58**, 481–496.

Schmitt, C. G., and W. P. Arnott, 1999: Infrared emission (500–2000 cm-1) of laboratory ice clouds. *J. Quant. Spectros. Radiat. Transfer*, **63**, 701–725.

Schmitt, C. G., and A. J. Heymsfield, 2009: The size distribution and mass-weighted terminal velocity of low-latitude tropopause cirrus crystal populations. *J. Atmos. Sci.*, **66**, 2013–2028.

Spichtinger, P., and K. M. Gierens, 2009: Modelling of cirrus clouds – Part 2: Competition of different nucleation mechanisms. *Atmos. Chem. Phys.*, **9**, 2319-2334.

Stephens, G. L., S. C. Tsay, P. W. Stackhouse, Jr., and P. J. Flatau, 1990: The relevance of the microphysical and radiative properties of cirrus clouds to climate and climatic feedback. *J. Atmos. Sci.*, **47**, 1742–1753.

Strapp, J. W., F. Albers, A. Reuter, A. V. Korolev, U. Maixner, E. Rashke, and Z. Vukovic, 2001: Laboratory measurements of the response of a PMS OAP-2DC. *J. Atmos. Oceanic Technol.*, **18**, 1150–1170.

Weickmann, H. K., 1947: *Die Eisphase in der Atmosphäre.* Library Trans. 273, Royal

Aircraft Establishment, Farnborough, 96pp.

Wendisch, M., P. Pilewskie, J. Pommier, S. Howard, P. Yang, A. J. Heymsfield, C. G. Schmitt, D. Baumgardner, and B. Mayer (2005): Impact of cirrus crystal shape on solar spectral irradiance: A case study for subtropical cirrus. *J. Geophys. Res.*, **110**, D03202.

Wendisch, M., P. Yang, and P. Pilewskie 2007: Effects of ice crystal habit on thermal infrared radiative properties and forcing of cirrus. *J. Geophys. Res.*, **112**, D08201.

World Meteorological Organization (WMO), 1975: *International Cloud Atlas, vol. I, Manual on the Observation of Clouds and Other Meteors*. WMO no. 407, WMO, Geneva.

Yoshida, Y., S. Asano, A. Yamamoto, N. Orikasa, and A. Yamazaki, 2004: Radiative properties of mid-latitude frontal ice-clouds observed by the shortwave and longwave radiometer-sondes. *J. Meteor. Soc. Japan*, **82**, 639–656.

Zhang, Y., A. Macke, and F. Albers (1999): Effect of crystal size spectrum and crystal shape on stratiform cirrus radiative forcing. *Atmos. Res.*, **52**, 59– 75.